Gradient Plasticity Model and its Implementation into MARMOT

Nuclear Energy Enabling Technology

PNNL-22702

Prepared for

U.S. Department of Energy

Nuclear Energy Enabling Technology Program

Erin Barker, Dongsheng Li, Hussein Zbib, Xin Sun

Pacific Northwest National Laboratory, Richland, WA 99352

August 2013

NEAMS Milestone Report M3MS-13PN0602051

SUMMARY

The influence of strain gradient on deformation behavior of nuclear structural materials, such as body-centered cubic (bcc) iron alloys has been investigated. We have developed and implemented a dislocation based strain gradient crystal plasticity material model. A mesoscale crystal plasticity model for inelastic deformation of metallic material, bcc steel, has been developed and implemented numerically. Continuum Dislocation Dynamics (CDD) with a novel constitutive law based on dislocation density evolution mechanisms was developed to investigate the deformation behaviors of single crystals, as well as polycrystalline materials by coupling CDD and crystal plasticity (CP). The dislocation density evolution law in this model is mechanism-based, with parameters measured from experiments or simulated with lower-length scale models, not an empirical law with parameters back-fitted from the flow curves.

In our current framework, geometrically necessary dislocations are introduced to take into consideration of strain gradient for the long range interactions. Two approaches have been proposed to incorporate the influence of strain gradient into the framework: the first one with analytical solution in a homogenization method, i.e., viscoplastic self-consistent (VPSC) model, the other one with user material subroutine in finite element method (FEM).

The mesoscale plasticity model is formulated to treat both long-range and short-range processes and interactions. Models for the evolution of mobile and immobile dislocations, as well as interstitial loops, and interaction hardening laws, are formulated based on quantifiable mechanisms from lower length scales, such as dislocation multiplication, annihilation, junction formation/breakage, and cross-slip in CDD. Long-range interactions, resulting from dislocation structures, will be treated within a dislocation-based strain gradient theory, compatible with dislocation theory and driven by densities represented as continuum fields.

Crystal plasticity has been implemented into MARMOT to increase the capability of the numerical solution framework for mechanical deformation behavior of nuclear structural materials. Combined with the lower length scale simulation capability in MOOSE, development in this capability will build up a multi-scale and multi-physics modeling architecture.

CONTENTS

LIST OF FIGURES

LIST OF TABLES

ACRONYMS

BCC	body-centered cubic
CDD	continuum dislocation dynamics
CP	crystal plasticity
Cr	chromium
CRSS	critical resolved shear stress
DD	dislocation dynamics
DDD	discrete dislocation dynamics
DOE	U.S. Department of Energy
FCC	face-centered cubic
Fe	iron
FS	Frank sessile
GND	geometrically necessary dislocation
MD	molecular dynamics
MWLSR	moving weighted least squares regression
Ni	nickel
PNNL	Pacific Northwest National Laboratory
R&D	research and development
SCCE-D	single crystal constitutive equations, based on dislocation density
SCCE-T	single crystal constitutive equations, for texture analysis
SSD	statistically stored dislocations
UMAT	user defined material routine
VPSC	viscoplastic self consistent

NUCLEAR ENERGY ADVANCED MODELING AND SIMULATION PROGRAM

Gradient Plasticity Model and its Implementation into MARMOT

1. INTRODUCTION

Plastic flow strength of nuclear structural materials depends on irradiated microstructures and other inherent properties. From the perspective of strain, it depends on strains and strain gradients. In the theory of dislocation dynamics, dislocations from plastic deformation may be categorized into: statistically stored dislocations (SSD) from bulk plastic strain and geometrically necessary dislocation (GND) from strain gradient. The strain gradient is attributed to the heterogeneity of the microstructure and geometric shape and size. In the early days of the gradient plasticity theory development, most of the studies focused on geometrically heterogeneous systems, such as sharp crack tip, thin wire torsion, indentation tests and so on.

In this study, the strain gradient will be focused on the heterogeneity from inherent microstructure, such as texture, precipitate, voids, and other heterogeneous microstructure contribution. The strain gradients are inversely proportional to the length scale of investigated system when the difference of strain is constant. Consequently, the contribution from strain gradient becomes apparent when the investigated length scale is small enough to reach the range of micrometer. Phenomenological theories of strain gradient plasticity were proposed by Fleck, Hutchinson and other front runners in the past decades, as summarized in several excellent reviews (Evans and Hutchinson, 2009; Fleck and Hutchinson, 1997; Fleck et al., 1994).

In our previous studies (Li et al., in preparation; Zbib et al., 2012), we have developed a multi-scale modeling framework to simulate the mechanical deformation behavior of nuclear structural materials including bcc iron alloys. The work flow of this multi-scale framework starts

from molecular dynamics (MD), to discrete dislocation dynamic (DDD), to continuum dislocation dynamics (CDD), to crystal plasticity (CP) model and FEM.

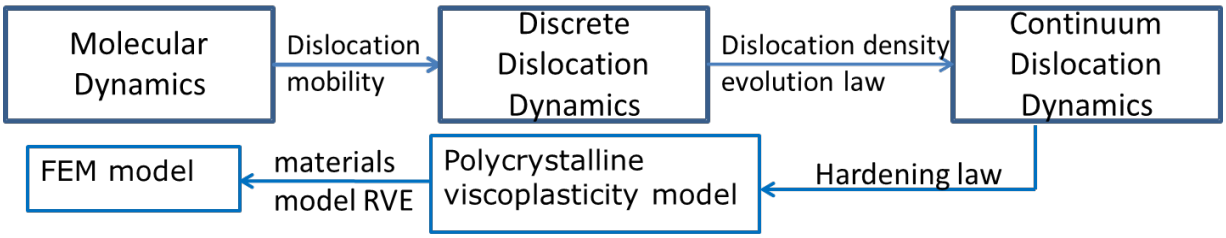

Figure 1. Scheme of multi-scale approach in mechanical flow prediction

Scale bridging in this framework has two types, tightly-coupled and loosely-coupled. The information pass from MD to DDD is loosely-coupled: dislocation mobility as a function of temperature and alloy composition is calculated from MD and passed in a suitable form to DDD model. The results gathered from the DDD simulations then lead to the evaluation of the dislocation density and critical resolved shear stress in Fe-Ni-Cr alloys as well as irradiation damage. The dislocation density evolution law is passed into CDD for mechanical behavior prediction. The bridging between CDD and polycrystalline viscoplasticity model is a tightly-coupled model. Finally, the results from CP are used as a material subroutine in FEM model.

To incorporate the influence of the strain gradient due to the sample geometry, length scale effect and heterogeneous microstructure, gradient plasticity has been utilized and added to the current framework. The updated workflow is illustrated in Figure 2 below:

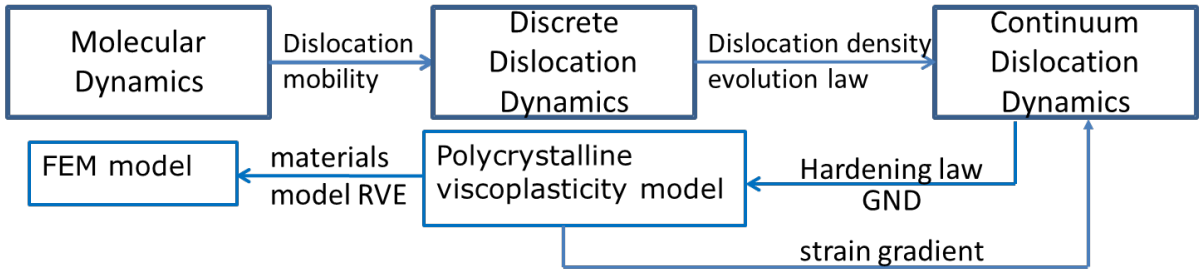

Figure 2. Work flow of multi-scale modeling predicting the plastic flow with long range interaction taken into consideration by strain gradient plasticity

In the early stage of strain gradient plasticity model, most models are phenomenological, treating the stress contributing the strain gradient as work conjugate higher order stresses in the form of couple stresses and double stresses, dealing with the strain gradient tensor in the form of deformation curvatures (Fleck and Hutchinson, 1993; Fleck and Willis, 2009a, b). The experimental evidences for the scale effect due to the strain gradient have been observed in the plastic flow of metals and ceramics. For example, the indentation hardness increases by a factor of 2 as the width of the indent is decreased from about 10 um to 1um (Stelmashenko et al., 1993). This is one example of Hall-Petch effect, the yield strength increases with the decrease of grain size. To capture the scale effect, or the grain boundary effect, we incorporated gradient plasticity.

The gradient plasticity theory used in our model is different from the fore-mentioned approach in two aspects: one is on the contribution of the strain gradient. In our model, two sources of strain gradients are taken into considerations: one is from sample geometry calculated by FEM model, the other one is from texture, calculated by polycrystalline viscoplasticity model. The other difference is our model is mechanism-based, not a phenomenological one. GND from strain gradient is incorporated in the model at the stage of dislocation dynamics.

Before the introduction of gradient plasticity, the elastic-plastic formulations developed since the 1960s are strain rate independent (Asaro and Rice, 1977; Hill, 1966; Mandel, 1965; Simo and Taylor, 1985) with yield surface defined by Hill's criterion. Later, a viscoplastic approach was proposed to achieve unique solutions to avoid the numerical multiple solutions from using strain rate sensitivity formulations (Asaro and Needleman, 1985; Hutchinson, 1976; Peirce et al., 1982). The essence of viscoplasticity theory is the hardening law, usually in a power law format, to relate the shear stress in each slip system to the shear strain rate. The advantage of the power law formulation is due to the derivation of viscoplastic potential with the capability to capture saturation effect at a high strain rate. Different versions of isotropic and anisotropic viscoplastic constitutive theories have been developed. Examples include MATMOD equations proposed by Miller (Henshall, 1996; Miller, 1976) to describe viscoplasticity function as a combination of a hyperbolic sine function and a power function.

Limited to small strain, back stress is used for kinematic hardening and a drag stress for isotropic hardening. Another example is Robinson's formulation, which is more complicated, using a back-stress, a drag stress, a yield stress, and a power function for the viscoplastic flow (Arnold and Saleeb, 1994). There are many other versions taking into consideration different factors. With the development of the theory of slip systems, hardening is decomposed into two parts: latent hardening and self hardening, both in the exponential function form to describe interaction between different slip systems (Asaro, 1983; Asaro and Needleman, 1985; Peirce et al., 1982). Nevertheless, most theories of resistance of shear stress evolution are empirical with the parameters determined by fitting the model to the experimental stress strain curves.

With the advent of dislocation dynamics and multi-scale modeling, alternative constitutive laws were proposed to introduce the knowledge generated from dislocation theory to the continuum plasticity framework. For example, Zbib and de la Rubia (Zbib and Diaz de la Rubia, 2002), Devincre (Devincre et al., 2008), Groh et al. (Groh et al., 2009), and Alankar et al. (Alankar et al., 2012b) proposed multi-scale approaches to establish a dislocation-based continuum model to incorporate discrete and intermittent aspects of plastic flows. In these approaches, strain hardening can be predicted through the modeling of mean free paths of dislocations. Other statistical aspects from dislocation dynamics simulation, such as dislocation densities, are used as internal state variables to capture deformation behavior of single crystals (Arsenlis and Parks, 2002; Ortiz et al., 2000). Another front noteworthy is Sandfeld's work (Hochrainer et al., 2007; Sandfeld et al., 2011) to bridge statistical continuum mechanics with dislocation dynamics by dislocation density tensor. Using a statistical description of dislocation interactions in terms of a Taylor-type yield stress and a back stress, which describes short-range repulsion of dislocations of the same sign, key features from discrete dislocation dynamics simulations were captured. The core of the interaction between the discrete dislocation dynamics and crystal plasticity is the evolution law of dislocation density.

Discrete dislocation dynamics (DDD) is a powerful tool that has been advanced significantly in the past decade (Canova et al., 1993; Ghoniem and Sun, 1999; Zbib et al., 1996, 1998). It has been used to explain the effect of irradiation on mechanical properties through large-scale simulations of interaction of numerous numbers of dislocations with defect clusters.

The work of Zbib and co-worker has shown that dislocations interactions with the elastic fields of nano-sized defect clusters in Cu and Pd lead to hardening followed by localized deformation and channel formation resulting from defect cluster annihilation by dislocations (Diaz de la Rubia et al., 2000; Ghoniem et al., 2000; Hiratani et al., 2002a; Hiratani et al., 2002b; Khraishi et al., 2002a; Li et al., 2010; Zbib et al., 2000). In the present work we investigate the effect of irradiation hardening in Fe-Ni-Cr systems. The goal is to predict the stress-strain curve and the critical resolved shear stress as a function of defect density, which is then used in the crystal plasticity model. However, in order for this method to work, a detailed knowledge of the dislocation mobility in an analytical form inside the materials is required. To effectively predict the mechanical behavior of the materials under irradiation at the continuum scale, critical information should be determined and progressively passed from one scale to another.

2. STRAIN GRADIENT CONTINUUM DISLOCATION DYNAMICS

The strain gradient CDD framework uses the strain gradient calculated from VPSC and FEM model to feed back for the GND and recalculate the flow stress. The principle of crystal plasticity was improved by introducing more physics-based mechanisms to substitute empirically derived constitutive and hardening laws. Based on the traditional kinematics of crystal plasticity, CDD also has three fundamental assumptions. First, the total deformation gradient F (Peeters et al., 2000; Schoenfeld et al., 1995) is assumed to be the product of two terms, elastic part F^e and plastic part F^p:

$$F = F^e F^p, \tag{1}$$

where, F^e is due to the elastic distortion of the lattice, and the plastic part F^p is due to the slip by the dislocation motion in the unrotated intermediate configuration. It evolution rate, $\dot{F}^p$, is expressed by the kinematic relation:

$$\dot{F}^p = L^p F^p \tag{2}$$

In the second assumption, the plastic velocity gradient L^p is expressed as the sum of a number of crystallographic slip rates, $\dot{\gamma}^{\alpha}$:

$$L^p = \sum_{\alpha=1}^{N} \dot{\gamma}^{\alpha} n^{\alpha} \otimes m^{\alpha} \tag{3}$$

where n^{α} and m^{α} are the vectors representing slip direction and slip plane normal of slip system α, and N is the number of slip systems.

In the third assumption here, the lattice deformation is equal to the elastic material deformation. The plastic velocity gradient consists of a symmetric part, strain rate D^P, and an antisymmetric part, total spin W^P:

$$D_{ij}^{p} = symm(L_{ij}^{p}) = \frac{1}{2} \sum_{\alpha=1}^{N} \dot{\gamma}^{\alpha} \left(n_i^{\alpha} m_j^{\alpha} + n_j^{\alpha} m_i^{\alpha} \right) \tag{4}$$

$$W_{ij}^{p} = symm(L_{ij}^{p}) = \frac{1}{2} \sum_{\alpha=1}^{N} \dot{\gamma}^{\alpha} \left(n_i^{\alpha} m_j^{\alpha} - n_j^{\alpha} m_i^{\alpha} \right) \tag{5}$$

Here, the plastic strain rate D^P determines the deformation behavior by updating the stress strain curve; while the total plastic spin W^P is used to update the orientation of crystals, texture, in polycrystalline materials.

Normally, the shear strain rate of each slip system α, $\dot{\gamma}^{\alpha}$, is determined by a strain-rate-dependent power law function of the form:

$$\dot{\gamma}^{\alpha} = \dot{\gamma}_0 \left| \frac{\tau^{\alpha}}{\tau_0^{\alpha}} \right|^{1/m} sign\left(\tau^{\alpha} \right) \tag{6}$$

where $\dot{\gamma}_0$ is reference strain rate, τ_0^{α} is the slip resistance of the slip system α, τ^{α} is the resolved shear stress along slip system α, and *m* is the rate sensitivity exponent. The parameters τ_0^{α} and m are obtained from experimental results using curve fitting.

In SCCE-T, the hardening law defines the evolution of critical resolved shear stress (CRSS) of slip system and is defined as follows (Asaro, 1983):

$$\dot{\tau}_0^\alpha = \sum_\beta h_{\alpha\beta}\dot{\gamma}^\alpha \tag{7}$$

where, $h_{\alpha\beta}$ is the hardening coefficient matrix with self-hardening and latent hardening components.

In contrast, in the CDD model discussed below, another form of power law is used by utilizing the results from DDD. Our constitutive law for the shear strain rate is based on the Orowan relation (Orowan, 1940):

$$\dot{\gamma}^\alpha = \rho_M^\alpha b v_g^\alpha \tag{8}$$

where ρ_M^α is the mobile dislocation density of slip system α, b is the Burgers vector, and v_g^α is the average dislocation glide velocity in slip system α.

In previously developed models, the dislocation glide velocity v_g^α, is expressed in a power law of resolved shear stress τ^α similar with shear strain rate of slip system α, τ_0^α:

$$v_g{}^\alpha = v_0\left|\frac{\tau^\alpha}{\tau_0^\alpha}\right|^{1/m} sign\left(\tau^\alpha\right) \tag{9}$$

Here the expression of dislocation glide velocity is improved to a general law using Kock-type activation enthalpy:

$$\mathrm{v_g^\alpha} = \begin{cases} \mathrm{v_D l_g \exp\left[-\frac{\Delta F_k}{kT}\left(1-\left(\frac{|\tau^\alpha|-\tau_0^\alpha}{\tau_P^\alpha}\right)^p\right)^q\right] sign(\tau^\alpha)} & \text{when } |\tau^\alpha| > \tau_0^\alpha \\ 0 & \text{when } |\tau^\alpha| \le \tau_0^\alpha \end{cases} \tag{10}$$

where l_g is the distance between the barriers. For a kink height, l_g is close to Burgers vector. V_D is the Debye frequency, and k is the Boltzmann constant. T is temperature, ΔF_k is Kock-type activation enthalpy, τ_P^α is the Peierls lattice resistance of the slip system α, and p and q are strain rate parameters. In this new proposed law, all parameters have physical meaning calculated from lower-length scale models. The slip resistance of slip system α, τ_0^α, is a summation of reference resistance τ_0 from lattice friction stress for moving dislocations;

resistance due to dislocation-defect interaction τ_d^{α}, mainly from irradiation; and resistance from dislocation hardening τ_{dh}^{α}:

$$\tau_0^{\alpha} = \tau_0 + \tau_d^{\alpha} + \tau_{dh}^{\alpha} \tag{11}$$

According to the Baily-Hirsch model (Ohashi, 1994), the resistance from dislocation hardening is slip resistance of statistically stored dislocations on other slip systems against moving ones on one specific slip system α. It is a function of interaction matrix of slip systems $\Omega^{\alpha m}$:

$$\tau_{dh}^{\alpha} = \sum_m \alpha b \mu \Omega^{\alpha m} \sqrt{\rho^m} \tag{12}$$

Here, b is Burgers vector, μ is shear modulus, α is a numerical factor on the order of 0.1, and ρ^m is the density of statistically stored dislocations accumulated on the slip system *m*.

The evolution rate of statistically stored dislocation density is related to the mean free path of moving dislocations on slip system α, L^{α} (Ohashi et al., 2007):

$$\dot{\rho}^{\alpha} = c\dot{\gamma}^{\alpha} / bL^{\alpha} \tag{13}$$

where $\dot{\gamma}^{\alpha}$ is the shear strain rate of slip system α, and *c* is a numerical constant of order 1. L^{α} is a function of dislocation density.

Assuming defects are distributed randomly for all slip systems, a modified dispersed barrier hardening model is used to express irradiation resistance τ_d^{α} from dislocation-defect interaction:

$$\tau_d^{\alpha} = \beta d \mu (\rho_d d)^n \tag{14}$$

where ρ_d is the defect density and *d* is the defect size. In a traditional dispersed barrier hardening model, *n*=0.5. In our proposed model, *n* is calculated directly from discrete DD.

In the previously proposed DD-based crystal plasticity models, the dislocation density evolution laws are either ignored or used a fitted curve to represent the evolution (as proposed by Kocks (Kocks, 1976)):

$$\dot{\rho}^{\alpha} = \frac{1}{b}\left(\frac{\sqrt{\sum_{\beta}^{n} \rho^{\beta}}}{k_a} - k_b \rho^{\alpha} \right) \left| \dot{\gamma}^{\alpha} \right| \tag{15}$$

where k_a and k_b are material parameters for dislocation generation and annihilation, respectively. This formulation was utilized by Wagoner et al. (Lee et al., 2010a) and Zbib et al. (Zbib and de la Rubia, 2002) on flow simulation of single crystals. Simulation results from this model will be compared with the mechanism-based CDD.

The evolution rate of the dislocation density is based on mechanisms that can be quantified from the discrete DD. Generally, the statistical stored dislocations can be divided into two types, mobile and immobile:

$$\rho_S^{\alpha} = \rho_M^{\alpha} + \rho_I^{\alpha} \tag{16}$$

In CDD, the evolution of mobile dislocation density is composed of six terms with different physical contribution. The first mechanism is from the multiplication and growth of resident dislocations and the production of new dislocations from Frank-Reed sources in slip system α:

$$\dot{\rho}_{M1}^{\alpha} = \alpha_1 \rho_M^{\alpha} \frac{\bar{\boldsymbol{v}}_{\boldsymbol{g}}^{\alpha}}{\bar{\boldsymbol{l}}^{\alpha}} \tag{17}$$

where α_1 is the dislocation multiplication coefficient, ρ_M^{α} is the mobile dislocation density distributed on slip system α, and $\bar{l}^{\alpha}$ is the mean free path of dislocations on slip system α.

The second mechanism captures the mutual annihilation of two mobile edge or screw dislocations with opposite signs in slip system α:

$$\dot{\rho}_{M2}^{\alpha} = -2\alpha_2 \boldsymbol{R}_c \left(\rho_M^{\alpha}\right)^2 \bar{\boldsymbol{v}}_{\boldsymbol{g}} \tag{18}$$

where α_2 is the dislocation annihilation coefficient and R_c is the capture radius for the dislocation annihilation event.

The third mechanism describes the transition of mobile type to immobile type due to the interaction between dislocations:

$$\dot{\rho}^{\alpha}_{M3} = -\alpha_3 \rho^{\alpha}_{M} \frac{\bar{\boldsymbol{v}}_{\boldsymbol{g}}}{\bar{\boldsymbol{l}}} \tag{19}$$

where α_3 is the immobilization parameter.

Conversely, the fourth mechanism is about the mobilization of immobile dislocations due to the breakup of junctions, dipoles, pinning parts, etc., at a critical stress condition:

$$\dot{\rho}^{\alpha}_{M4} = \alpha_4 \left(\frac{\left|\boldsymbol{\tau}^{\alpha}\right|}{\boldsymbol{\tau}^{*}} \right)^{r} \rho^{\alpha}_{I} \frac{\bar{\boldsymbol{v}}^{\alpha}_{\boldsymbol{g}}}{\bar{\boldsymbol{l}}} \tag{20}$$

where α_4 is the mobilization parameter.

The fifth mechanism considers cross-slip, the phenomena where screw dislocation segments on one slip plane move to another glide plane during plastic deformation. Extensive reviews of cross-slip in experiments and simulations have been given by Jackson (Jackson, 1985) and Püschl (Püschl, 2002). Cross-slip has been observed in experimental work and simulated using molecular dynamics, dislocation dynamics, and other low-length scale models (Alankar et al., 2012a; Bitzek et al., 2008; Püschl, 2002). In large-length scale, cross-slip was incorporated in a continuum model in an empirical way, either assuming a recombination distance or a dissociation energy (Püschl, 2002). There is a disconnection in the modeling influence of cross-slip on deformation behavior across different length scales. In most continuum texture models, cross-slip has been ignored. In our model, evolution of mobile dislocation due to cross-slip is defined as below:

$$\dot{\rho}^{\alpha}_{M5} = \alpha_5 \sum_{\beta=1}^{N} \boldsymbol{P}^{\alpha\beta} \rho^{\beta}_{M} \frac{\bar{\boldsymbol{v}}^{\alpha}_{\boldsymbol{g}}}{\bar{\boldsymbol{l}}} \tag{21}$$

where α_5 is the cross-slip parameter, N is the number of cross-slip planes available for each Burgers vector, e.g. in fcc N=2, and in bcc N=12. $P^{\alpha\beta}$ is the cross-slip probability matrix; the components of this matrix are either 0, -1 or +1; $\boldsymbol{P}^{\alpha\beta} = 0$ means no cross-slip of dislocations from system β to system α, $\boldsymbol{P}^{\alpha\beta} = +1$ indicates cross-slip of dislocation from β to α, and $\boldsymbol{P}^{\alpha\beta} = -1$ means that the system α lost dislocations to system β by cross-slip. In this setup,

cross-slip is treated as a stochastic process and, therefore, we use a Monte-Carlo type analysis similar to that used in the discrete dislocation dynamics for cross-slip (Rhee et al., 1999; Zbib et al., 1998). We emphasize the introduction of this stochastic term that makes it possible to predict the anisotropic behavior of single crystals for different loading directions as shown in the next section. More details regarding the implementation of cross-slip in the continuum dislocation theory are given in Li et al (Li et al., in preparation).

The sixth mechanism is similar to the second one, also annihilation, but between mobile and immobile type dislocations:

$$\dot{\rho}_{M6}^{\alpha} = -\alpha_6 \boldsymbol{R}_c \ \rho_I^{\alpha} \rho_M^{\alpha} \bar{\boldsymbol{v}}_g^{\alpha} \tag{22}$$

Combining all of the preceding considerations, the evolution rate of mobile dislocations is:

$$\dot{\rho}_M^{\alpha} = \alpha_1 \rho_M^{\alpha} \frac{\bar{v}_g^{\alpha}}{\bar{l}} - 2\alpha_2 R_c \left(\rho_M^{\alpha}\right)^2 \bar{v}_g - \alpha_3 \rho_M^{\alpha} \frac{\bar{v}_g}{\bar{l}} + \alpha_4 \left(\frac{\left|\tau^{\alpha}\right|}{\tau^*}\right)^r \rho_I^{\alpha} \frac{\bar{v}_g^{\alpha}}{\bar{l}} + \alpha_5 \sum_{\beta}^{N} p^{\alpha\beta} \rho_M^{\beta} \frac{\bar{v}_g^{\alpha}}{\bar{l}} - \alpha_6 R_c \rho_I^{\alpha} \rho_M^{\alpha} \bar{v}_g^{\alpha} \tag{23}$$

The aforementioned mechanisms of mobile dislocations evolution, including Eq. (19), (20), and (22), also involve the immobile dislocations. Based on these, the evolution rate of immobile dislocation density is:

$$\dot{\rho}_I^{\alpha} = \alpha_3 \rho_M^{\alpha} \frac{\bar{v}_g^{\alpha}}{\bar{l}} - \alpha_4 \left(\frac{\left|\tau^{\alpha}\right|}{\tau^*}\right)^r \rho_I \frac{\bar{v}_g^{\alpha}}{\bar{l}} - \alpha_6 R_c \rho_I^{\alpha} \rho_M^{\alpha} \bar{v}_g^{\alpha} \tag{24}$$

The predicted mobile and immobile dislocation density are used to calculate the total dislocation density using Eq. (16), which in turn predicts the resistance from dislocation hardening according to Eq. (12).

The evolution rate of statistically stored dislocation density along slip system α is treated as the summation of the two dislocation density evolution rate above, similar to Eq. (16):

$$\dot{\rho}_S^{\alpha} = \dot{\rho}_I^{\alpha} + \dot{\rho}_M^{\alpha} \tag{25}$$

In our current framework, another kind of dislocation, geometrically necessary dislocation, is introduced to taken into consideration of strain gradient for the long distance interaction. The evolution rate of total dislocation, $\dot{\rho}$, is composed of two parts, evolution rate of GND, $\dot{\rho}_G$ and the evolution rate of SSD, $\dot{\rho}_S$:

$$\dot{\rho} = \dot{\rho}_S + \dot{\rho}_G = \sum \dot{\rho}_S^{\alpha} + \dot{\rho}_G \tag{26}$$

In traditional strain gradient theory, the magnitude of the plastic strain gradient is of the order of the average shear strain in the crystal divided by the local length scale λ of the deformation field. The strain gradient is γ/λ, where γ is macroscopic plastic shear strain. In approximate terms,

$$\rho_G = \frac{4\gamma}{b\lambda} \tag{27}$$

And the flow stress, or macroscpic shear yield stress is approximately

$$\tau = CGb\sqrt{\rho_G + \rho_S} \tag{28}$$

where G is the shear modulus, b is the magnitude of the Burger's vector, and C is the constant taken to be 0.3 by Ashby (1970).

In our framework, this geometrically necessary dislocation is calculated out by:

$$\left\|\rho_G^{\alpha}\right\| = \sqrt{\left(\rho_{G,edge}^{\alpha}\right)^2 + \left(\rho_{G,screw}^{\alpha}\right)^2} \tag{29}$$

where $\rho_{G,edge}^{\alpha} = -\frac{1}{\tilde{b}}\frac{\partial \gamma^{(n)}}{\partial \xi^{(n)}}$ and $\rho_{G,screw}^{\alpha} = \frac{1}{\tilde{b}}\frac{\partial \gamma^{(n)}}{\partial \zeta^{(n)}}$

Here ξ and ζ denote, respectively, directions parallel and perpendicular to the slip direction on the slip plane.

3. STRAIN GRADIENT FIELD CALCUALTED FROM POLYCRYSTALLINE VISCOPLASTICITY MODEL

To simulate the deformation behavior of polycrystalline materials, we used a viscoplasticity self-consistent model (Lebensohn and Tomé, 1994). As mentioned previously, fully plastic deformation is assumed, and it is further asserted that the deformation takes place through shear and is independent of the hydrostatic stress. This allows a five dimensional vector space to be used to in the formulation of inelastic deformation in terms of conjugate deviatoric stress and strain rate tensors. Interchanging two components of the stress and strain convention adopted by Lequeu et al. (Lequeu et al., 1987), the stress and strain rate vectors from second order tensor are given by

$$\{\sigma'\} = \sqrt{2}\left\{\frac{(\sigma_{33}-\sigma_{11})+(\sigma_{33}-\sigma_{22})}{2\sqrt{3}}, \frac{\sigma_{22}-\sigma_{11}}{2}, \sigma_{23}, \sigma_{13}, \sigma_{12}\right\}^{T} \tag{25}$$

$$\{\dot{\varepsilon}\} = \sqrt{2}\left\{\frac{(\dot{\varepsilon}_{33}-\dot{\varepsilon}_{11})+(\dot{\varepsilon}_{33}-\dot{\varepsilon}_{22})}{2\sqrt{3}}, \frac{\dot{\varepsilon}_{22}-\dot{\varepsilon}_{11}}{2}, \dot{\varepsilon}_{23}, \dot{\varepsilon}_{13}, \dot{\varepsilon}_{12}\right\}^{T} \tag{26}$$

The scalar product of these two vectors gives the stress power, i. e.,

$$\sigma'_k \, \dot{\varepsilon}_k = \sigma'_{ij} \, \dot{\varepsilon}_{ij} \tag{27}$$

where it is understood that the sum on subscript k is over the range 1,2,...,5. Inelastic deformation occurs only when a slip and/or twin system is active. Both slip and twin systems are characterized by two vectors: the slip systems unit normal vector **n** and the unit vector **b** in the slip direction. Again, twinning is treated in this formulation as pseudo-slip, with the same formulation of the kinematics as crystalline slip.

Each grain of the polycrystal has the kinematic relation provided by CDD. The VPSC model couples the strain-rate and the stress in each grain with the average strain rate and stress of the polycrystal (Lebensohn and Tomé, 1993). Each grain is regarded as an inhomogeneity embedded in the homogeneous equivalent medium (HEM) having a viscoplastic compliance $\mathbf{M}^{(tg)}$ and a reference strain rate $\dot{\mathbf{E}}^{0}$, whose behavior is identical to the average of the polycrystal with a viscoplastic compliance $\mathbf{M}^{c(tg)}$ and a reference strain rate $\dot{\boldsymbol{\varepsilon}}^{0}$. This

inhomogeneity has a local stress field when a uniform stress is applied to the HEM. Using the Eshelby formalism, the inhomogeneity is replaced by an 'equivalent inclusion' having the same moduli as the polycrystal, subjected to a fictitious transformation strain rate $\dot{\boldsymbol{\varepsilon}}^{*}$.

The overall viscoplastic compliance moduli of the grain, $M^{(\mathrm{sec})}$, can be calculated in a self-consistent iterative way, as the HEM is assumed to describe the average behavior of the aggregate. This forces the weighted average of stress and strain rate over the grains to coincide with corresponding macroscopic values.

Texture evolution is simulated by enforcing the polycrystal deformation through successive incremental steps. These are obtained by imposing a macroscopic strain rate $\dot{\mathbf{E}}$ during the time interval Δt, with a guess value at each step used for the strain rate $\dot{\boldsymbol{\varepsilon}}$ in each grain. The first deformation step uses a Full Constraints guess. The stress is then calculated with each following step using the values from previous steps as the starting guesses. The macroscopic secant modulus $\mathbf{M}^{(\mathrm{sec})}$ is estimated using the Voigt average, $\mathbf{M}^{(\mathrm{sec})-1} = \left\langle \mathbf{M}^{\mathrm{c}(\mathrm{sec})-1} \right\rangle$ for the first step, with the following steps using preceding values to derive the next estimate. This modulus is then used to calculate the Eshelby tensor, **S**, the interaction tensor, $\mathbf{M}^{0c}$, and the accommodation tensor, $\mathbf{B}^{\mathrm{c}}$. The average $\left\langle \mathbf{M}^{\mathrm{c}(\mathrm{sec})}\mathbf{B}^{\mathrm{c}} \right\rangle$ is used as an improved guess for $\mathbf{M}^{(\mathrm{sec})}$, with repeated iterations until the average coincides with the input tensor, under a certain tolerance. This value is then used to calculate the macroscopic stress

$$\boldsymbol{\Sigma}' = \mathbf{M}^{(\mathrm{sec})-1}\dot{\mathbf{E}} \tag{28}$$

Each grain is then allowed to reorient due to slip and twinning, following a convergence criterion. The lattice rotation rate for each grain is given by

$$\dot{\omega}_{ij} = \dot{\Omega}_{ij} + \Pi_{ijkl}S^{-1}_{klmn}\dot{\varepsilon}^{0}_{mn} - \sum_{s}\frac{1}{2}(b^{s}_{i}n^{s}_{j} - b^{s}_{j}n^{s}_{i})\dot{\gamma}^{s} \tag{29}$$

where $\dot{\Omega}$ is the anti-symmetric component of the macroscopic distortion rate, Π is the reorientation of the associated ellipsoid, and ***S*** is the antisymmetric component of the plastic distortion rate (plastic spin); Π is proportional to the difference between the strain rate of the grain and that of the polycrystal. Tiem et al. (Tiem, 1986) showed that for the elastic inclusion case, Π increases with ellipsoid distortion. The modeling of the grain orientation will then use

the Volume Transfer Scheme as described by Lebensohn and Tome (Lebensohn, 1991; Tome, 1991) for twinned volume fractions. The polycrystal is represented as a discrete set of orientations. These orientations are fixed, but their representative volume fractions evolve during deformation. The Euler space is partitioned regularly in equiaxed cells or bins of 10 degrees on dimension of Euler angle. The orientations coincide with the centers of the cells. A certain volume fraction of the material is assigned to each cell, corresponding to the initial texture. The reorientation of lattice orientation that drives texture evolution during inelastic deformation is visualized as displacements in Euler space of the represented points. If the cell as a whole displaces rigidly and partially overlaps neighbors, then the volume fraction of material in the overlap is subtracted and transferred to the neighbors. This is repeated every iteration, providing gradual texture evolution.

4. RESULTS AND DISCUSSION

4.1 Low Length Scale Models Providing Dislocation Density Evolution Law

While this work focus on continuum dislocation dynamics, some example of molecular dynamics and discrete dislocation dynamics simulation results is presented here to demonstrate the flow of the information from microscale to mesocale.

In the dislocation dynamics framework, the mobility of a screw dislocation is considered to be a small constant fraction of the mobility of the edge dislocation therefore, if the mobility of either an edge or a screw dislocation is known, the mobility of the other type can be calculated in terms of this mobility (Gilbert et al., 2011; Marian and Caro, 2006). Therefore, if the mobility of the edge dislocation is known, the mobility of the screw can be also found. Results for the dislocation mobility in iron alloys have been reported elsewhere in (Lim et al., 2011; Mastorakos et al., 2010; Mastorakos et al., 2011a; Mastorakos et al., 2011b). The Embedded Atom Method (EAM) (Daw and Baskes, 1983) and potentials developed in (Bonny et al., 2009; Mendelev et al., 2003; Stukowski et al., 2009) for the pure iron, Fe-Cr and Fe-Ni respectively were used. In

particular, the dislocation mobility in a series of Fe-Ni-Cr systems at different temperatures has been simulated using molecular dynamics.

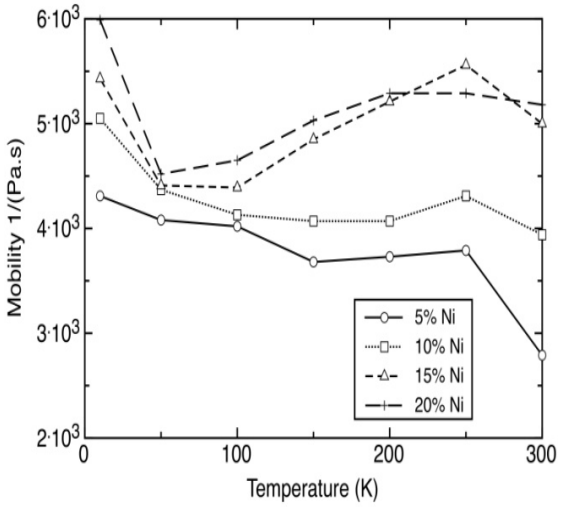

Figure 3. Dislocation mobility as a function of the temperature in Fe-Ni system, with concentration of nickel or chromium was varied from 5% to 20%

Representative results for the edge dislocation mobility, in Fe-Ni alloy with nickel composition at 0%, 10%, 15% and 20%, are shown in Figure 3. The results from these simulations lead to power law relationship for the dislocation mobility of the form $M = a_0 + m/\sqrt{T - T_0}$ where M is the mobility, T the absolute temperature, a_0, and m are numerical parameters. a_0 varies between 3771 to 5135, and m between 321 to 367. The results reveal that edge dislocation mobility is higher in the Fe-Ni systems compared to the α-Fe and increases as the Ni concentration increases. On the other hand, the dislocation mobility inside the Fe-Cr is comparable to that of pure iron although it still is about 5% higher. The higher edge mobility of the alloys compared to the pure Fe is backed by experimental observations that show a higher density of screw dislocations in alloys because the edge dislocations are very fast and disappear at the surface of the specimen (Guyot and Dorn, 1967; Nadgorny, 1988). This is also backed by other simulations of screw dislocations mobility showing that it is lower than the edge mobility (Gilbert et al., 2011; Marian and Caro, 2006)

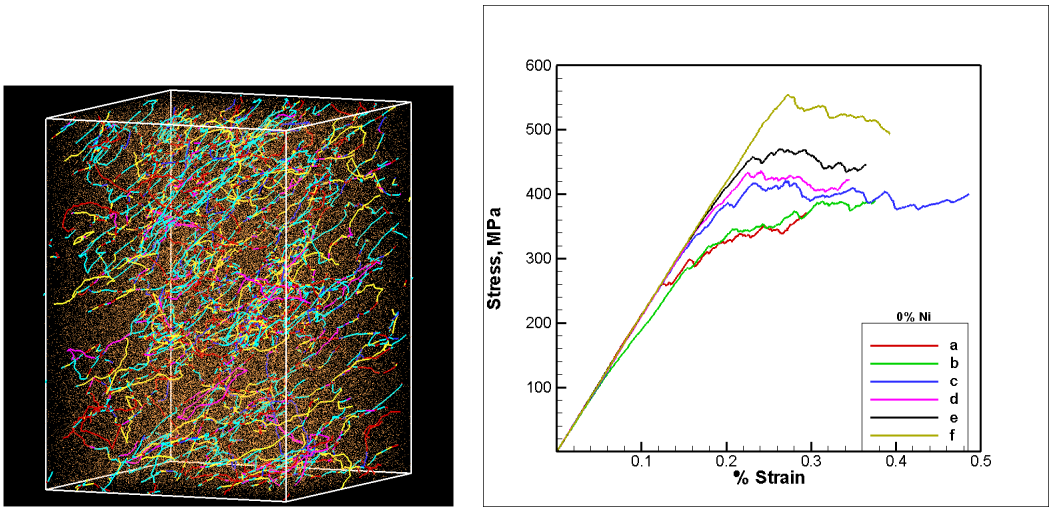

a) b)

Figure 4. a) Dislocation-defect structure after plastic deformation. b) Stress-strain curves simulated by DDD for iron single crystal at different defect densities (a:0, b:2×10^{22}, c:5×10^{22}, d: 7×10^{22}, e: 1×10^{23} , f: 2×10^{23}.)

Dislocation mobilities of iron alloys calculated from molecular dynamics are used in conjunction with the dislocation dynamics simulations to predict the evolution of dislocation density as a function of alloy and defect density. The DD simulation unit cell, shown in Figure 4(a), is a 4.5×4.5×5.97 μm^3 cube cell that contains an initial density of Frank-Read sources distributed randomly on the primary (Hiratani et al.) slip planes. In the simulations, periodic boundary conditions were imposed. The cell is loaded in tension with a constant strain rate of 100/s. The effect of irradiation is accounted for by mapping into the DD box a spatial distribution of FS loops with density ranging from 10^{20} /m^3 to 10^{24} /m^3. The loops are 1 to 3 nanometers in radius, and the radius is randomly generated to fall within the specified interval. The model also generates Frank-Read sources, represented as finite dislocation segments pinned at ends, lying on (Hiratani et al.) glide planes, and Burgers vectors of the type <111>.

Dislocation density evolution and the mobile-dislocation-related CRSS are predicted from discrete DD. The dislocation structure shown in Figure 4a is composed mainly of extended dislocations of screw character, resulting from the fact that the mobility of the screw dislocation is three orders of magnitude less than the edge. As the dislocations sweep through

the cloud of the FS loops, some of the loops get annihilated, depending on their interaction energy with the sweeping dislocations as discussed before by various authors (Ghoniem et al., 2000; Hiratani et al., 2004; Khraishi et al., 2002a).

This results in the formation of defect-free channels, and subsequently causes a drop in the flow stress as deduced from the stress-strain curves. Figure 4(b) demonstrates the initial deformation behavior of pure iron with different defect densities. In all cases, the stress initially increases linearly until it is high enough for dislocations to overcome internal barriers and the pinning effect of the defects, which arises only from dislocation-FS loops elastic interactions. As the dislocations propagate and interact with the defects, their interaction energy with the defect at a critical distance can cause defect absorption within the dislocation core, which, in turn, leads to a drop in stress (Khraishi et al., 2002b) and a decrease in defect density.

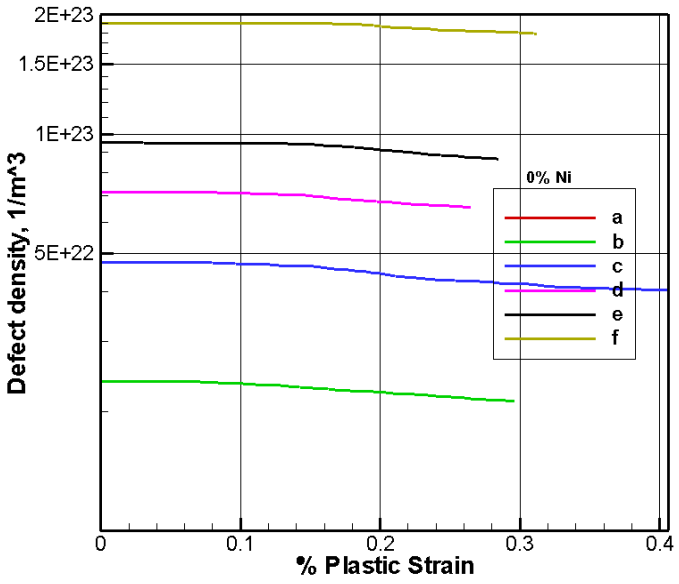

(a)

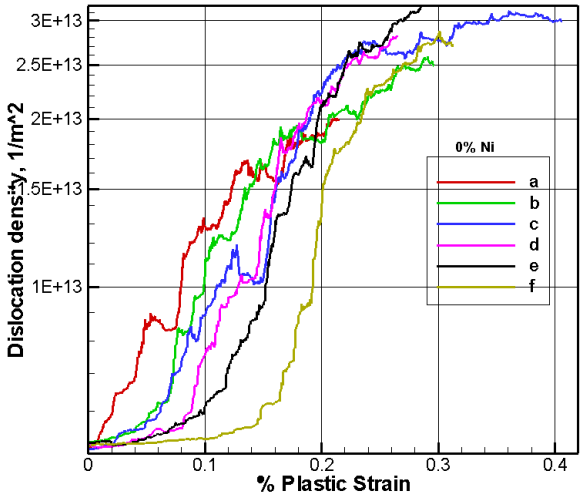

(b)

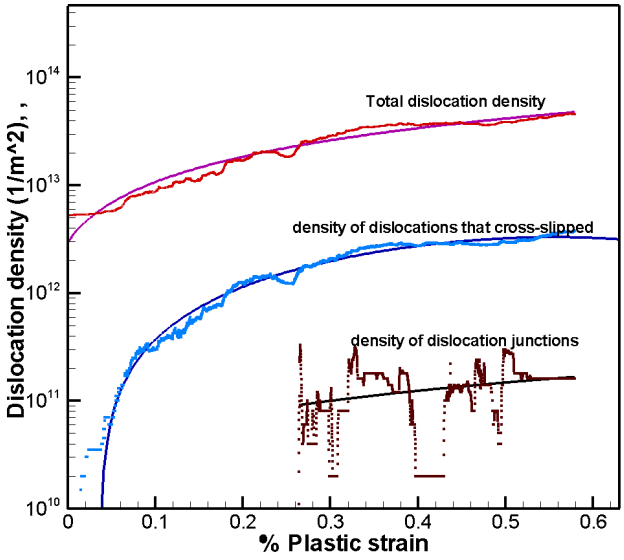

(c)

Figure 5. Discrete dislocations dynamics results: Evolution of defect density (a) and dislocation density (b) for iron alloy with 5%Ni concentrations at different initial irradiation defect density: (a:0, b:2×10^{22}, c:5×10^{22}, d: 7×10^{22}, e: 1×10^{23} , f: 2×10^{23}.) , (c) evolution of total dislocation density, cross-slip segments and dislocations junctions.

Figure 5(a) shows typical DD results for the evolution of the defect density with deformation. In all cases, the defect density remains unchanged during the elastic loading as expected. As the stress becomes high enough to cause the dislocations to move, the dislocations interact with the defects and some of them get annihilated, causing a decrease in the defect density. In the meantime, the dislocation densities in Fe-Ni alloys with different initial defect density generally increase with deformation, as shown in Figure 5(b). Dislocations are further categorized and recorded during the deformation process. Figure 5(c) provides the detailed information of evolution of cross slip and junction. This information will be used in calculating the dislocation density evolution parameters $\alpha_{1\text{-}6}$.

4.2 CDD in Predicting Mechanical Properties of Fe Single Crystal

With the predicted dislocation density evolution from DDD, CDD is used in predicting the flow behaviors of Fe single crystals. The advantage of this framework is the physical meaning of all the parameters in the mesoscale model. With consideration of cross-slip, anisotropic Peierls stress for different slip systems, CDD can predict the strength and deformation behavior of single crystals with higher fidelity. The parameters for pure α-Fe used are listed in Table 1, partially built upon Lee's previous works (Lee et al., 2010b; Lim et al., 2011).

Table 1 . List of parameters used in the continuum dislocation dynamics model

Symbol	Denotation	Value
M	Shear modulus	80GPa
N	Poisson's ratio	0.3
C_{11}	Anisotropic elasticity constant	242 GPa
C_{12}	Anisotropic elasticity constant	150 GPa
C_{44}	Anisotropic elasticity constant	112 GPa
γ_0	Reference strain rate	4×10^{-5} m/s
M	Strain rate sensitivity	0.012
A	Baily-Hirsch hardening coefficient	0.4
B	Magnitude of Burger vector	2.54×10^{-10}m
τ_0	Peierls stress (internal friction)	11.0MPa
B	Irradiation hardening coefficient	0
α_1	Mobile dislocation multiplication coefficient	0.02

α_2	Mobile-mobile dislocation annihilation coefficient	1.0
R_c	Critical radius for annihilation in units of Burger vector	15
α_3	Immobilization parameter, mobile to immobile	0.002
α_4	Mobilization parameter, mobile to immobile	0.002
α_5	Cross-slip coefficient	0.018
α_6	Mobile-immobile annihilation coefficient	1.0

One point should be emphasized here: the parameters are either experimentally measured (such as μ and C_{11}) or calculated from the discrete DD (e.g., the parameters in the mechanisms of dislocation density evolution law, α_1, α_2, etc.). Along with the advantages already mentioned, there are four other salient points in the proposed framework. The first is the application of cross-slip, the second is the anisotropic Peierls stress, the third is the updated strain rate sensitivity law with information of dislocation density, and the fourth is the capability to predict irradiation hardening by introducing hardening due to interaction between dislocation and defects.

We compared the CDD prediction results with the experimental results measured by Keh et al. (Keh, 1965) and simulation results from SCCE-T and SCCE-D. The CDD parameters used in Table 2 are from predicted results using DDD and lower-length scale models. The parameters used in SCCE-T and SCCE-D are from back-fitting the mechanical testing results. 12 (1 1 0)[1 1 1] and 12 (1 1 2)[1 1 1] slip systems in body center cubic (BCC) crystal systems were considered for crystallographic slip. In the initial state, mobile and immobile defect density are considered the same, and are distributed uniformly along 24 slip systems.

Using uniaxial tension stress strain curve of Fe single crystals along [100] direction as a benchmark in SCCE-T and SCCE-D, the simulated flow curves along [100], [011] and [-348] are shown in Figure 6. The process of back-fitting constitutive parameters in SCCE-T and SCCE-D are detailed in previous works (Lee et al., 2010a). Using the parameters fit from [100] direction, SCCE-D and SCCE-T both agree with experimental data along [100], even better than the prediction results from CDD. However, using the same parameters to simulate the flow curve along [011] direction, SCCE-D underestimates and SCCE-T overestimates the stress. When applied on [-348] direction, SCCE-D overestimates more than 50% of the experimental results

while SCCE-D overestimated more than 100% of the experimental data. Predicted results using CDD agree well with experimental data along all three directions.

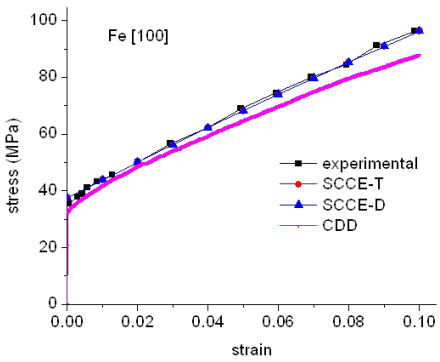

(a)

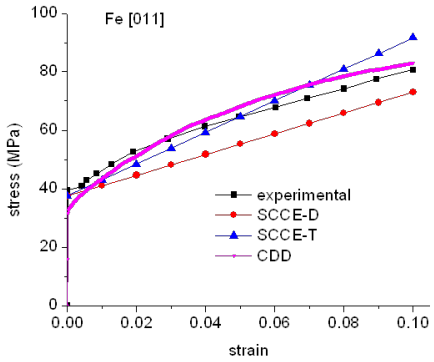

(b)

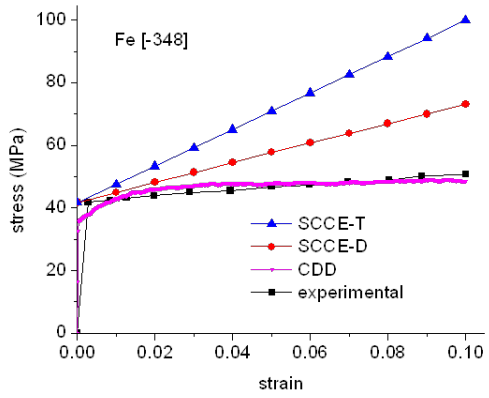

(c)

Figure 6. Comparison of experimental stress strain curves and simulated results from SCCE-T, SCCE-D and CDD models for iron single crystal with uniaxial tensile loading direction along (a) [100] (b) [011] and (c) [-348] directions. The constitutive law parameters for SCCE-T and SCCE-D are back-fit to the [100] results.

On the other hand, if the constitutive parameters are back-fitted using the experimental data along [-348] direction, SCCE-T and SCCE-D only work in the benchmark case, [-348] shown here in Fig. 7(c). But they will not work in the other directions, as shown in Fig.

7(a) and (b). The large deviation demonstrates the limitations of empirical constitutive equations without scientific mechanisms in background support.

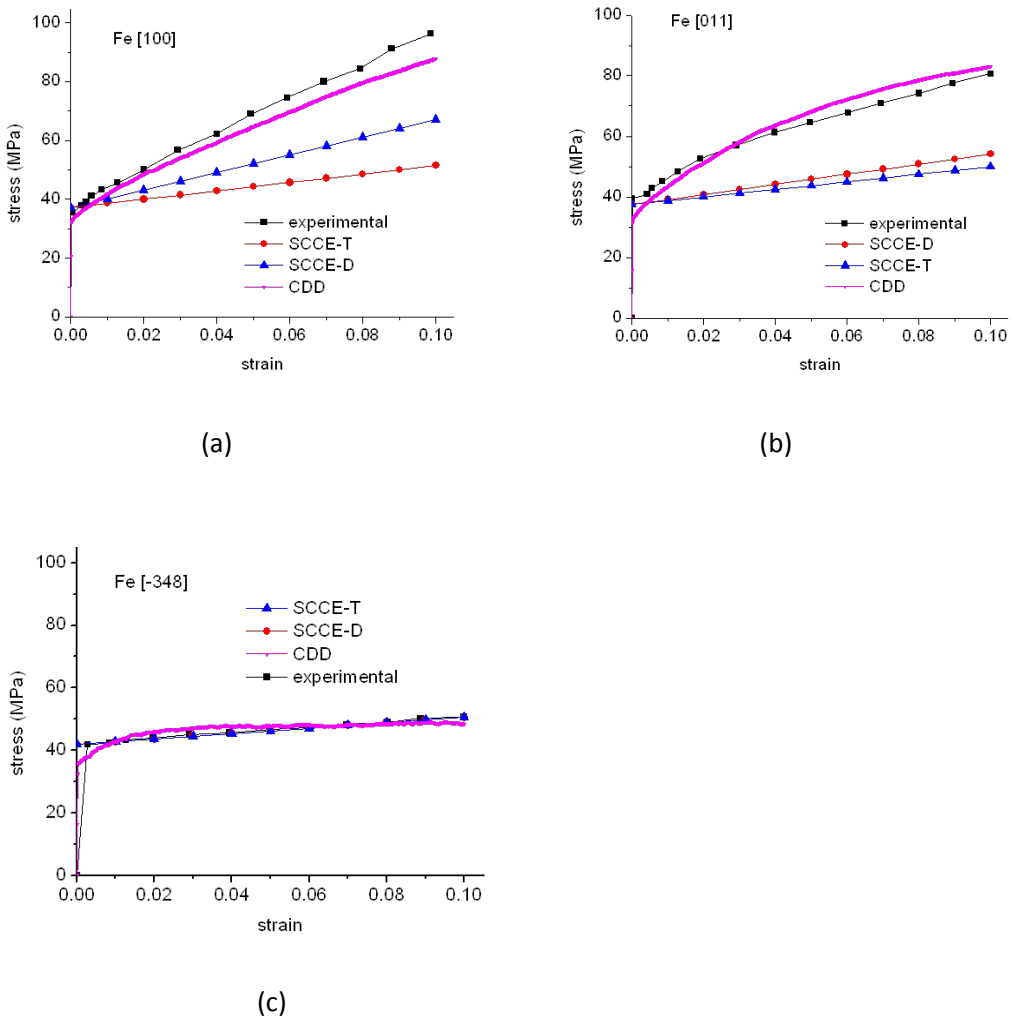

Figure 7. Comparison of experimental stress strain curves and simulated results from SCCE-T, SCCE-D and CDD models for iron single crystal with uniaxial tensile loading direction along (a) [100] (b) [011] and (c) [-348] directions. The constitutive law parameters for SCCE-T and SCCE-D are back fit to the [-348] results.

Experimental data of single crystal iron demonstrated large behavior differences when uniaxially stretched along different directions. The yield stresses are similar for all directions, around 35 to 40 MPa. Contrasting to the large strain hardening with the stress increased dramatically to over 90MPa along [100] direction, there is little strain hardening when stretched along [-348] direction. This is due to the number of slip systems activated. Fig. 8

shows the evolution of mobile dislocation density (Fig. 8a) and total dislocation density (Fig. 8b). With the increase of strain, the dislocation density along (-211)[111] increases with small vibration due to annihilation and transfer to immobile type. Dislocation densities along all the other directions keep almost constant to the end. Combined with the information from immobile dislocation, the total dislocation density increased smoothly with strain, compared with the evolution of mobile dislocation density along (-211)[111].

Some parameters used in CDD may be measured directly from experiments; some from DDD and MD simulations. Parameters like cross slip coefficient is a parameter hard to measure from experiment, while difficult to simulate directly since it is sensitive to the dislocation microstructure. It is the same to Peierls stress anisotropic factor. A parameter sensitivity study has been carried out to conduct the comparison of the variance with different CDD parameters. Experimental stress strain curve of iron single crystal is used to verify the choice of parameters. The table below shows a part of the parameter fit results we obtained for the variance:

Table 2. Variance of the simulation results from experimental stress strain curve for two CDD parameters

parameters	Peierls stress anisotropic factor=1	1.5	2	2.5	3.5	4	4.5
cross slip coefficient=0	0.514	0.6211	0.6153	0.6056	0.6056	0.6056	0.6056
0.004	0.5094	0.5353	0.4708	0.4641	0.4637	0.4626	0.4655
0.008	0.4407	0.3864	0.3239	0.3189	0.3177	0.3229	0.3199
0.012	0.2976	0.2138	0.1749	0.1861	0.1739	0.1725	0.1779
0.016	0.1284	0.0562	0.064	0.0523	0.0434	0.0472	0.049
0.02	0.0525	0.0334	0.0433	0.0448	0.0436	0.0397	0.0343

For a robust simulation, cross lip coefficient of 0.02 and Peierls stress anisotropic factor of 1 are the best from the simulated results demonstrated in Table 2.

4.3 Prediction of Deformation Behavior and Texture Evolution using CDD-CP

Constitutive law based on dislocation density evolution predicted from continuum dislocation dynamics is introduced into the viscoplasticity model to solve the boundary condition loading stress and strain. This is in turn passed into the continuum dislocation dynamics model to solve the evolution of mobile and immobile dislocation density in each crystal and the corresponding slip resistance for each slip system.

CDD-CP is applied in a polycrystalline iron alloy with bcc crystal structure and random texture, composed of 100 crystals. (100), (110) and (111) pole figures of the selected system is demonstrated in Fig. 8. The maximum texture intensity in them is lower than 1.3 times random.

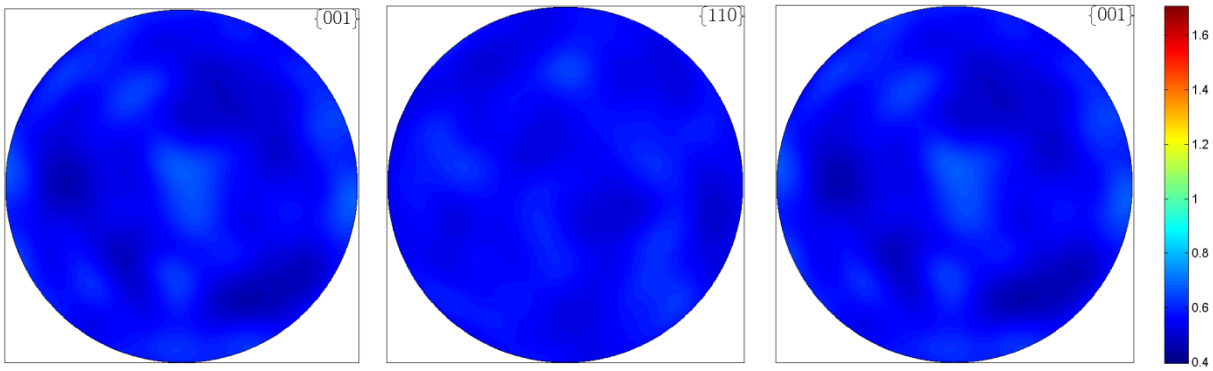

Figure 8. (a) 100, (b) 110, and (c) 111 pole figures of simulated bcc iron sample with random texture.

Under uniaxial tension, the predicted stress strain curve up to a strain of 10% is presented below, with features of strain hardening and saturation hardening captured.

The stress flow in Fig. 9 demonstrated yielding around a strain of 0.02. After that, strain hardening started to saturate. Texture evolution during uniaxial tension is shown in Fig. 10:

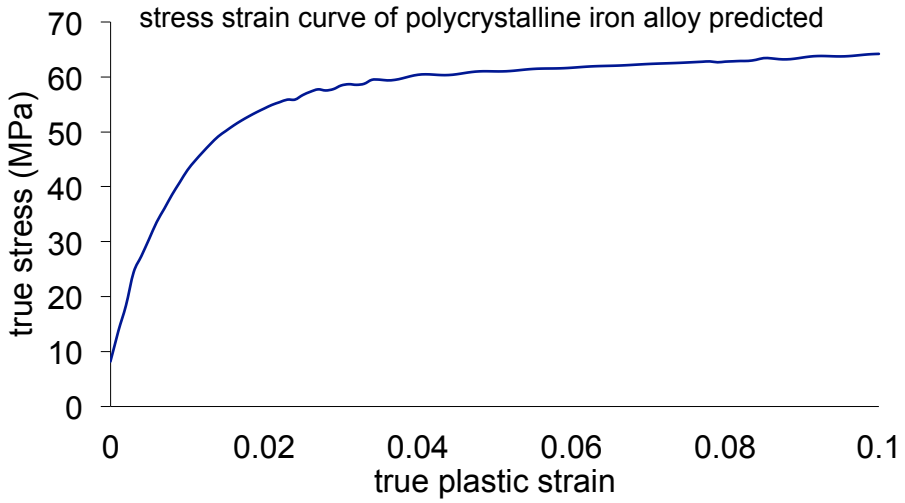

Figure 9. Predicted stress strain curve of the random texture iron using CDD-CP model.

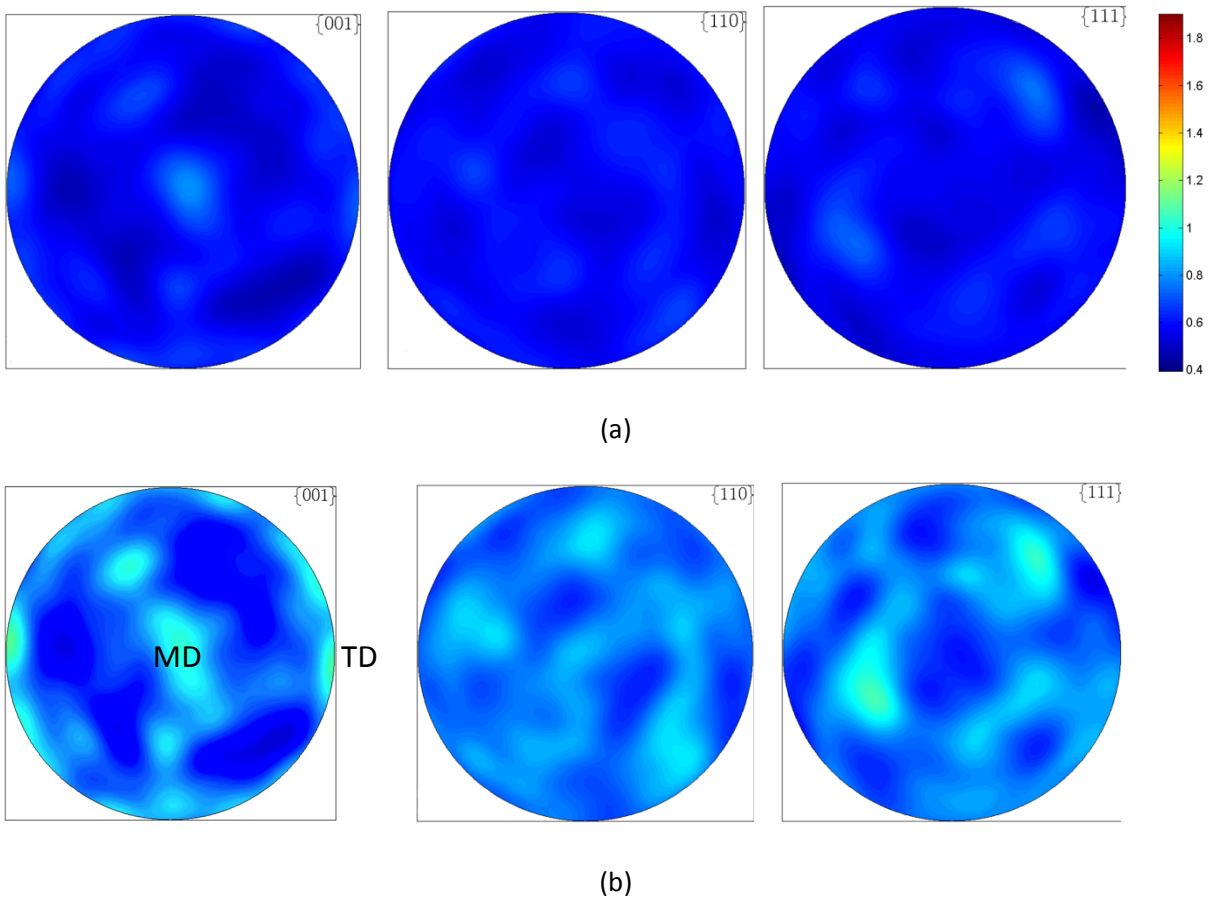

Figure 10. Predicted (100), (110) and (111) pole figures of random bcc iron alloys under uniaxial tension at strain of (a) 2% and (b) 10%.

In the (100) pole figure, a texture component with (001) aligned along machine direction (tensile here) appeared at a strain of 2% and strengthened at 10%.

A simulated microstructure with single crystal grid was generated with random texture. Each grid represented a single crystal with different orientation. The heterogeneous microstructure introduce different strain field, with a strain gradient field. Below is a work flow for the closely coupled crystal plasticity model and CDD. In the gradient plasticity CDD informed CP, the feed from CP has strain gradient added while the return from CDD to CP has more information on the GND, SSD and updated constitutive law.

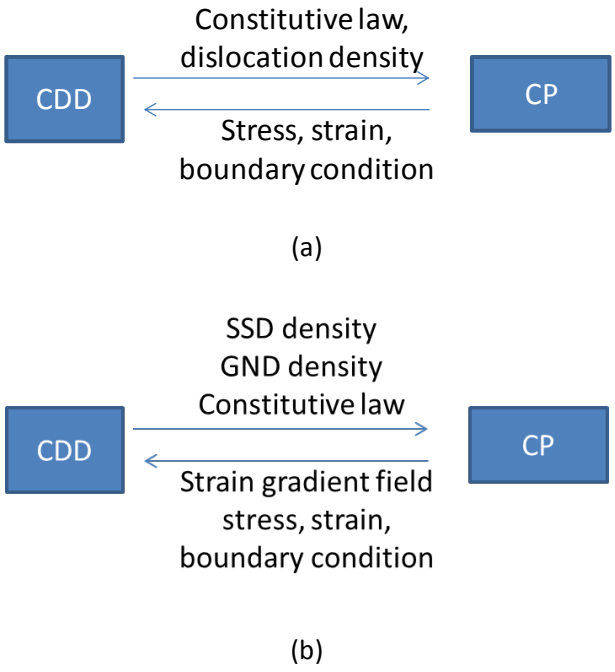

Figure 11. Scheme of data flow in closely coupled CDD and CP (a) without (b) with long distance interaction considered.

The simulation results for the strain of a random microstructure are illustrated in the figure below. There are 10×10 single crystals, the strain of each grain, or grid, is represented by a color grain when the sample is uniaxial tensioned to a different effective strain in Fig. 12.

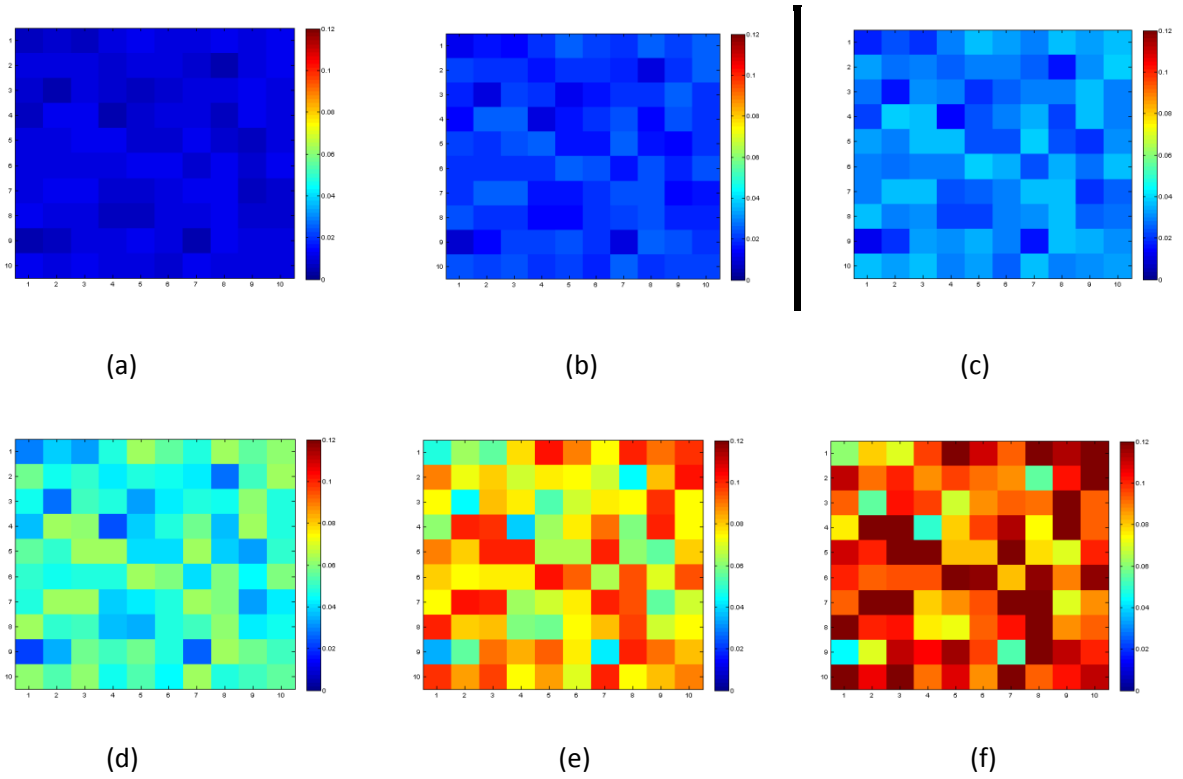

(a) (b) (c)

(d) (e) (f)

Figure 12. Strain field of random textured polycrystalline agglomerate after uniaxial tensioned to a strain of (a) 0.1, (b) 0.2 (c) 0.3 (d) 0.5 (e) 0.8 and (f) 1.0.

Correspondingly, the strain gradient calculated from the above strain field is illustrated in the figure below.

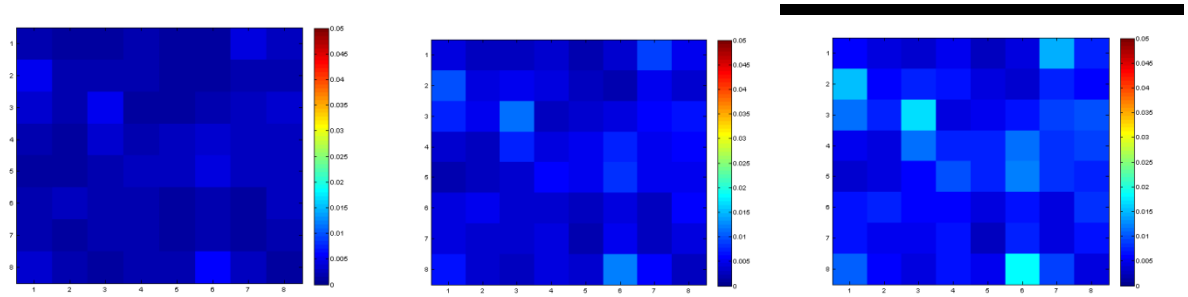

(a) (b) (c)

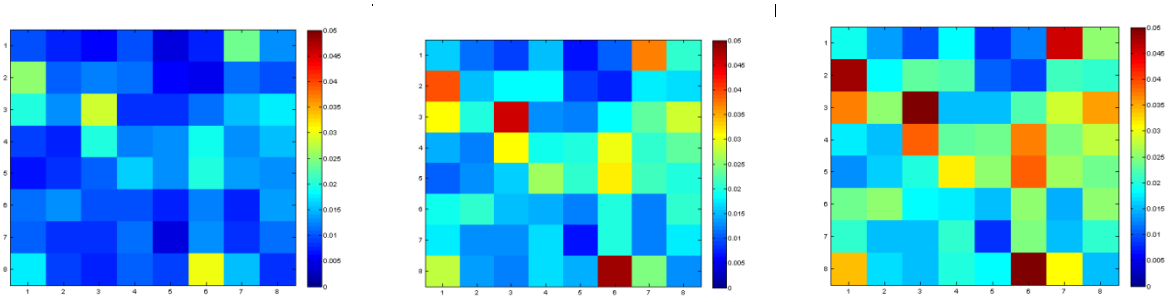

(d) (e) (f)

Figure 13. Strain gradient field of random textured polycrystalline agglomerate after uniaxial tensioned to a strain of (a) 0.1, (b) 0.2 (c) 0.3 (d) 0.5 (e) 0.8 and (f) 1.0

When a large system with 2000 crystals, a grid of 40×50, is used, the distribution of strain is more uniform, as shown in figure below.

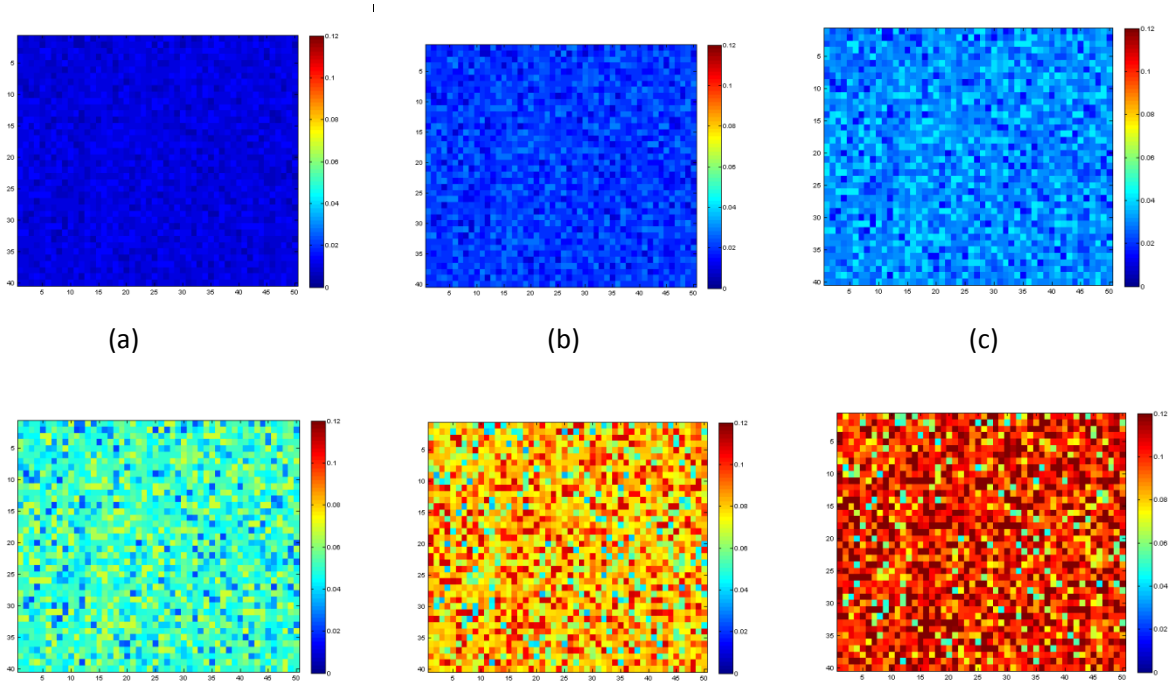

(a) (b) (c)

(d) (e) (f)

Figure 14. Strain field of random textured polycrystalline agglomerate with 2000 grains after uniaxial tensioned to a strain of (a) 0.1, (b) 0.2 (c) 0.3 (d) 0.5 (e) 0.8 and (f) 1.0

The responding strain field calculated is illustrated below:

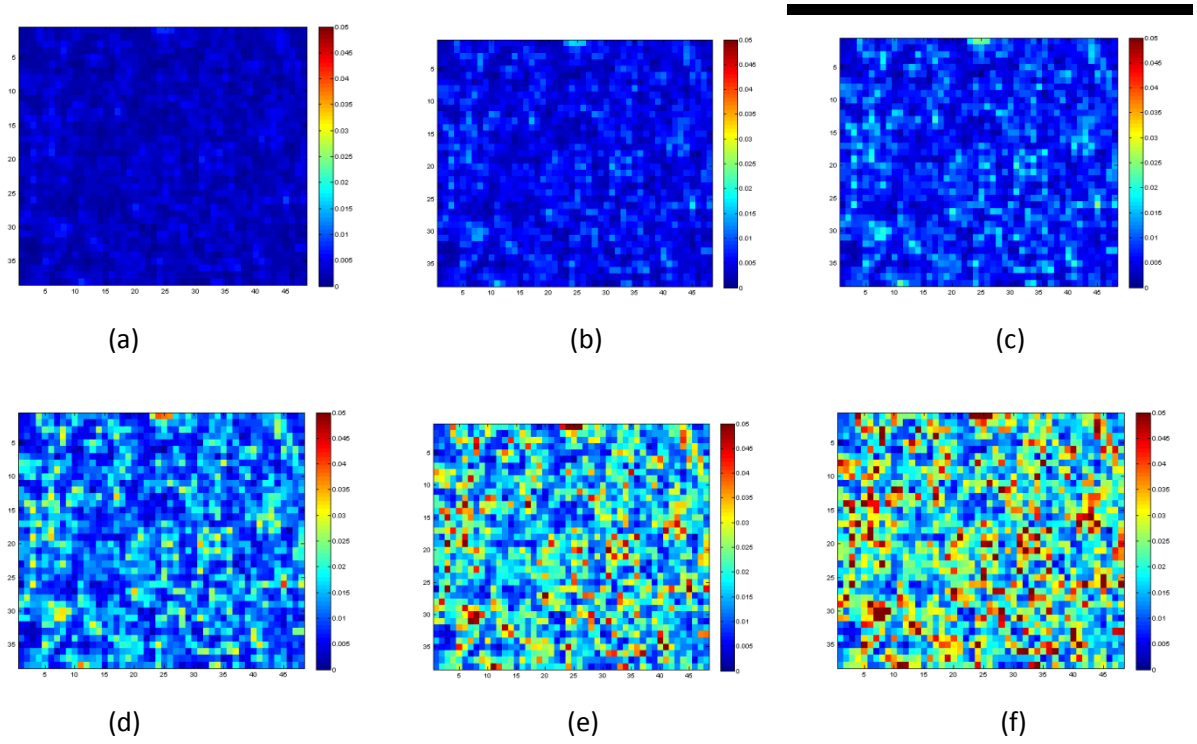

Figure 15. Strain gradient field of random textured polycrystalline agglomerate with 2000 grains after uniaxial tensioned to a strain of (a) 0.1, (b)0.2 (c) 0.3 (d) 0.5 (e) 0.8 and (f) 1.0

Further comparison with experimental data is necessary for validation.

5. IMPLEMENTATION OF CRYSTAL PLASTICITY IN MARMOT

A simplified version of the CDD model was also implemented as a material calls within MARMOT, a multi-physics, finite element simulation tool focused on the mesoscale. MARMOT is implemented using the MOOSE framework from INL (Tonks, 2012).

As discussed in Section 2, our constitutive law for the shear strain rate is based on the Orowan relation (Orowan, 1940):

$$\dot{\gamma}^{\alpha} = \rho_M^{\alpha} b v_g^{\alpha} \tag{30}$$

where ρ_M^α is the mobile dislocation density of slip system α, b is the Burgers vector, and v_g^α is the average dislocation glide velocity in slip system α.

As in previously developed models, for our simplified CDD model the dislocation glide velocity v_g^α, is expressed in a power law of resolved shear stress τ^α similar with shear strain rate of slip system α, τ_0^α:

$$v_g{}^\alpha = v_0 \left| \frac{\tau^\alpha}{\tau_0^\alpha} \right|^{1/m} sign\left(\tau^\alpha\right) \tag{31}$$

It should be noted, this is a deviation from our CDD model implementation in the VPSC framework. The dislocation glide velocity expression shown in Eq. (10) will be implemented in future work. As shown in Eq. (11), the slip resistance of slip system α, τ_0^α, is a summation of reference resistance τ_0 from lattice friction stress for moving dislocations; resistance due to dislocation-defect interaction $\tau_d{}^\alpha$, mainly from irradiation; and resistance from dislocation hardening τ_{dh}^α:

$$\tau_0^\alpha = \tau_0 + \tau_d^\alpha + \tau_{dh}^\alpha \tag{32}$$

The dislocation hardening term, τ_{dh}^α, is the resistance of statistically stored dislocations on each slip system from moving dislocation on the system *n*.

$$\tau_{dh}^\alpha = \sum_m \alpha b \mu \Omega^{\alpha m} \sqrt{\rho^m} \tag{33}$$

where $\Omega^{\alpha m}$ is the interaction matrix of the slip systems and ρ^m is the summation of the mobile and immobile dislocation densities. For this initial simplified implementation, the dislocation density term excludes the strain gradient influence.

For the VPSC implementation, defects are assumed to be distributed randomly for all slip systems and a modified dispersed barrier hardening model (Eq. 14) is used to express irradiation resistance τ_d^α from dislocation-defect interaction. For this simplified

implementation, the defect density and defect size are held constant and available as model inputs. Therefore τ_d^α , becomes constant for a given simulation.

The statistically stored dislocations required by the dislocation hardening term can be generally divided into two types, mobile and immobile, as shown in Eq. (16). The evolution equations for both types of dislocations are shown in Eq. (23) and (24), respectively. See Section 2 for further discussion of the evolution equations.

5.1 MARMOT Implementation

The CDD implementation in MARMOT begins from the strong form of the governing equations on the domain Ω and boundary $\Gamma = \Gamma_{l_i} \bigcup \Gamma_{g_i}$ as follows:

$$\nabla \cdot \sigma + b = 0 \text{ in } \Omega \tag{34}$$

$$u = g \text{ in } \Gamma_g \tag{35}$$

$$\sigma \cdot n = l \text{ in } \Gamma_l \tag{36}$$

where σ is the Cauchy stress tensor, u is the displacement vector, b is the body force, n is the unit normal to the boundary, g is the prescribed displacement on the boundary, and l is the prescribed traction on the boundary. The weak form of the residual becomes:

$$\Re = \left(\sigma, \nabla \phi_m\right) - \left\langle l, \phi_m \right\rangle - \left(b, \phi_m\right) = 0 \tag{37}$$

where $\left(\cdot\right)$ and $\left\langle \cdot \right\rangle$ represent volume and boundary integrals, respectively. The Jacobian required by Newton's method for solving the residual equation can be expressed as the following, when ignoring the boundary terms:

$$\Im = \left(\frac{\partial \sigma}{\partial \nabla u}, \nabla \phi_m \right) \tag{38}$$

The stress is a nonlinear function of the strain during plastic deformation. This function is defined by crystal plasticity theory (see section 2, Eq. 1-5) and our simplified CDD constitutive model as described in the previous section.

There are a series of material base classes available through MARMOT. The CDD model was implemented using the FiniteStrainMaterial base class that is part of TensorMechanicsMaterial implemented in ELK, another component of MOOSE. All material base classes provide methods for initializing state properties, calculating incremental strain updates, and calculating the current stress. The CDD implementation utilizes the existing strain update method while overriding the initialization and stress calculation methods.

The method computeStrain follows the algorithm outlined by Rashid (Rashid, 1993) for calculating the incremental deformation gradient. The method computeQpStress is left pure virtual for any material that inherits to override with the desired constitutive relationship. Finally, the method initQpStatefulProperties can be overridden and expanded to initialize additional state variables as needed.

The computeQpStress implementation used here follows the patterns seen elsewhere in MARMOT.

$$\begin{aligned}
&\varepsilon^e = \varepsilon_n^e + \Delta\varepsilon \\
&D^p = \varepsilon_n^p \\
&\text{solveStressResidual}(\sigma_n, \Delta\varepsilon, C_{ijkl}, D_{n+1}^p, \sigma_{n+1}) \\
&\varepsilon_{n+1}^p = RD_{n+1}^p R^T \\
&\sigma_{n+1} = R\sigma_{n+1}R^T
\end{aligned} \tag{39}$$

where the elastic strain, ε^e, and plastic strain, ε^p, are first updated. Then the stress residual is solved. This method updates values of the plastic strain rate, D_{n+1}^p, and stress, σ_{n+1}. Before exiting, rotations are applied. The bulk of the constitutive model is implemented within the method solveStressResidual.

solveStressResidual integrates the CDD constitutive model in an incremental manner using a Newton Raphson implementation. Given the complexity of the constitutive model this is

implemented in two levels. An internal loop solves the stress residual while an external loop updates and solves the slip resistance residual.

5.2 Plan for Strain Gradient Addition to MARMOT Implementation

The incorporation of a strain gradient term to the CDD model will enable this crystal plasticity model to more accurately capture the effects of long-range dislocation interactions. While the evolution equations for immobile dislocations presented above account for short-range interactions among dislocations, these evolution equations do not at present include the effects of long-range interactions. Long-range forces also act to impede dislocation motion. In the vein of the work of Fleck and Hutchinson (Fleck and Hutchinson, 1997; Fleck et al., 1994; Fleck and Willis, 2009a), and following the work of Zbib and Aifantis (Zbib and Aifantis, 1992, 2003), we introduce the use of a strain gradient term to capture long-range geometrically necessary dislocations (GNDs).

Long-range forces resulting from GNDs are an important source of hardening. In the formulation used here, the gradient of the plastic strain with respect to both the normal and tangential in-plane directions is calculated, representing edge and screw GNDs, respectively. The plastic strain values are equivalent to the slip in each crystallographic slip system. Multiplied by a length scale term, these strain gradient values are used to update the mean free dislocation glide path term:

$$\rho_{\mathrm{I}}^{\alpha} = \frac{\Delta\gamma^{\alpha}}{bL^{\alpha}}, \text{ where } L^{\alpha} = \frac{c^{*}}{\sqrt{\sum_{\beta} \omega^{\alpha\beta}\left(\rho_{I}^{\beta} + \rho_{GND}^{\beta}\right)}} \tag{40}$$

where, L^{α} is the updated mean free path term. The mean free path term is used in the evolution of immobile dislocation equations. Inclusion of the strain gradient term allows for a more accurate hardening model.

Numerically the strain gradient term is acquired as the derivative of strain values collected at the integration points of several elements. It is critically important that the strain gradient term depend on strain values from more than a single element. Methods that calculate the

strain gradient within a single element through a second derivative of the shape functions, such as work by Busso et.al. (Busso et al., 2000), fail to capture the long-range nature of GND interactions. While these methods are computationally compact, these formulations limit the range of GND interactions. The potential for the introduction of numerical artifacts also exists within these single element methods. Furthermore these methods, which calculate the strain gradient within a single element, produce a mesh-dependent strain gradient value.

Employed here is a formulation that links the strain gradient term to strain values across a cumulative volume of elements. The use of multiple elements in the calculation of the strain gradient term enables a mesh-independent strain gradient: the long-range effects captured in this manner are not bound by the size of elements.

Concerns about the continuity of the strain are an issue with which the strain gradient calculation must deal. Previous work in the field has made use of meshless methods or higher order (C^1) formulations to reach across element boundaries. As discussed below in greater detail, care is taken to address continuity when using strain values from multiple elements.

Original efforts to implement a strain gradient term into the CDD model focused on leveraging previous work within the context of an ABAQUS UMAT at Washington State University (WSU). Unfortunately direct porting of the strain gradient calculation from the UMAT was not possible: the absence of key utility functions in MOOSE and the heavy computational effort required by the WSU UMAT method forced the exploration of C^1 formulations. Thermodynamic consistency and straightforward integration with existing CDD formulations were of primary consideration in selecting and deriving an appropriate C^1 formulation. For developmental ease, the isotropic hardening small strain C^1 formulation is presented below.

The previous implementation utilized a moving weighted least squares regression method. Through the use of a computationally expensive ABAQUS utility function, strain values from across multiple elements are used to calculate the strain gradient. Integration points from multiple elements are selected within a radius of capture, and the strain values from these selected integration points are numerically collected with the utility function. These collected

strain values are fitted to a second order polynomial curve using a Moving Weighted Least Squares Regression (MWLSR); the moving description refers to the use of the radius of capture to select integration points. For each integration point in the model a new selection process is performed by sweeping a sphere, defined by the radius of capture, around the integration point.

Following the work of Abu Al-Rub et al. (Abu Al-Rub et al., 2007), a weighting function is used to assign more importance to the fit of strain values from integration points near the center of the sphere. As a result of this method strain values within the same central element are weighted more heavily by the MWLSR method than strain values from outer elements. The reasoning of the use of the weighting function is threefold: 1) the weighting function provides a more stable numerical solution, 2) the weighting function in some way mimics the $1/r$ behavior of long-range dislocation interactions, and 3) the weighting function provides a limited ability to address continuity issues. As noted by de Borst et al. (De Borst and Pamin, 1996), only the discretization of the gradient term requires C^1-continuous shape functions. In the vein of meshless methods, the weighting function is an attempt to provide continuity in the strain gradient calculation despite the use of strain values from several C^0 elements.

The derivative of the second-order MWLSR produced curve, with respect to the normal and tangent directions, is taken as the strain gradient for each of the slip systems in the crystal. Using this method two strain gradient terms are calculated for each slip system, increasing the computational effort required.

This procedure, used to calculate the strain gradient in ABAQUS, is extremely computational expensive. The obvious main source of computational load is the MWLSR, which is completed twelve times for every integration point in the mesh of an FCC crystal system. Contributing factors also include the calculation of selected integration points via the radius of capture and the use of the utility function to call the strain values at all of the selected integration points. The error introduced by the MWLSR process should also not be disregarded; this error is carried forward into the crystal hardening.

Although the strain gradient term would be the most useful in polycrystalline simulations, the computational effort required by this implementation severely limits the number of crystals that can be included in an ABAQUS simulation.

In light of these complications with the strain gradient calculation method used in ABAQUS, we elected to explore the option of a higher order C^1 formulation. The decision to move to the C^1 formulation was affirmed by the absence of a MOOSE utility function to numerically collect strain values from several integration points. The higher order C^1 formulation proposed for implementation into the CDD model in Marmot is more strongly rooted in thermodynamic principles. Following the strain gradient reformulation done by Abu Al-Rub, this C^1 formulation is admissible under the Clausius-Duhem Inequality when non-local quantities are properly considered.

Since the C^1 formulation is continuous in both displacement and strain, this formulation has the potential to be more accurate than MWLSR method currently employed in the ABAQUS UMAT at WSU. Since the strain is continuous across neighboring elements, it is not necessary to use a weighting function to force continuity for the strain gradient calculation. The C^1 method could also eliminate the error resulting from the curve-fitting, if the additional degrees of freedom (moments) are adequately treated.

In the literature comparisons (Huang et al., 2004) of C^0 and higher order formulations have noted that the primary difference between these two categories of formulations is seen at interfaces. Based on perturbation work performed by (Shu et al., 2001), the effect of higher order formulations is evident only in a thin layer near boundaries. While many groups have often neglected this thin boundary layer, capture of this boundary layer could prove to be useful in future multi-scale modeling efforts. We would argue that use of the more complex C^1 formulation is a responsible choice for enabling future model development.

Finally, and critically, the C^1 formulation would not require the use of a computationally intensive utility function to call strain values from multiple elements. Rather the C^1 formulation would make use of the additional degrees of freedom available in the third-order Hermite element to calculate the strain gradient.

The challenges associated with a C^1 formulation should not be overlooked. As discussed by Zhang et al. (Zhang et al., 2013) in a phase field application, a C^1 formulation significantly increases the stiffness matrix bandwidth. This increased bandwidth results in a longer simulation wall clock time. At present, only a limited number of hermite elements are available in the libMesh library; therefore, only simple geometries can be studied with a higher order formulation for now. Proper treatment of the higher order terms introduced in a C^1-continuous yield condition is not trivial. Any development work considering a C^1 formulation should carefully weight the potential increased accuracy against the certain increase in computational expense.

5.2.1 Theoretical Overview of Higher Order Strain Gradient Formulation

A brief overview of the theory behind the proposed C^1 formulation to calculate the strain gradient is presented here. Several excellent reviews of the current field of strain gradient work are available in the literature (Abu Al-Rub et al., 2009; Evers et al., 2004; Fleck and Hutchinson, 1997; Huang et al., 2004; Roters et al., 2010); however, we only discuss key concepts for brevity's sake.

We motivate the use of the strain gradient to account for GNDs through the definition of the Nye's tensor (Arsenlis and Parks, 1999; Bassani, 2001; Nye, 1953). The Nye's dislocation density tensor is a general representation of the *i*-component of the net Burger's vector related to the GNDs with *j* direction:

$$\alpha_{ij} = \sum_{\beta} \rho_{GND}^{\beta} b_i^{\beta} t_j^{\beta} \tag{41}$$

, where ρ_{GND}^{β} is the GND density, b_i^{β} is the Burger's vector, and t_j^{β} is the tangent unit vector for the ## slip system. The use of the generalized Nye's tensor allows for the accurate non-uniform distribution of GNDs through the crystal geometry. Following (Arsenlis and Parks, 1999; Bassani, 2001; Fleck and Hutchinson, 1997), the definition for the Nye's dislocation density

tensor can be written as a function of the second derivative of displacement through application of the Stokes' theorem.

$$\alpha_{ij} = e_{jkl} u^p_{i,lk} \tag{42}$$

Because of the choice to use the Hermite third-order element, the second derivative of displacement $u^p_{i,lk}$ could be accessed directly via the second derivative variable class in MOOSE. However, to ensure thermodynamic consistency, the second derivative of displacement can be related to an effective plastic strain variable through the plastic strain

$$\dot{p} = \sqrt{\frac{2}{3}\dot{\varepsilon}^p_{ij}\dot{\varepsilon}^p_{ij}} = \sqrt{\frac{2}{3}\dot{u}^p_{ij}\dot{u}^p_{ij}} \tag{43}$$

Substituting the definition of the effective plastic strain from Eq. 43 into Eq 42, we derive the Nye's dislocation density tensor as a function of effective plastic strain

$$\alpha_{ij} = \sum_{\beta} p^{\beta}_{k} e_{jkl} \mu^{\beta}_{il} \tag{44}$$

as in Gao et.al. (Gao et al., 1999). The introduction of the effective strain gradient to incorporate additional isotropic hardening has been employed by several groups in various forms (Acharya and Bassani, 2000; Muhlhaus and Aifantis, 1991; Polizzotto et al., 1998). Gurtin (Gurtin, 2000, 2003) treated dependence on plastic strain gradients through microforce balances and supplemented classical boundary conditions with non-local boundary conditions from the flow rule.

Within the CDD model represented by equation Eq. 40, the scalar accumulation of the GND density is used. By taking the square root of the square of equations Eq. 41 and Eq. 44, we propose that the accumulated density of GNDs can be calculated from the effective plastic strain by setting these two equations equal to each other:

$$\alpha = \sqrt{\alpha_{ij}\alpha_{ij}} = b\rho_{GND} = \sum_{\beta} \sqrt{\rho^{\beta}_{,k}\rho^{\beta}_{,k}}\,, \tag{45}$$

when interactions among dislocations on different slip systems are neglected. A similar approach to an effective strain gradient is employed by Gao (Gao et al., 1999). Eq. 45 demonstrates the calculation of the density of the GNDS from the gradient of the effective strain. This calculated effective GND density can then be used to update the mean free dislocation glide path (Eq. 40 within the larger CDD model. The use of an accumulated GND density value is in contrast to the tensor approach used by Akasheh et.al. (Akasheh, 2007 #100) although this difference in approach should be evident only in the numerical implementation.

The effective strain gradient model we use here, differs from previous approaches (Acharya and Bassani, 2000; Muhlhaus and Aifantis, 1991; Polizzotto et al., 1998) in the inclusion of the effective strain gradient in the internal power expression. The principle of virtual power is used to derive the microforce balance in the vein of Gurtin (Gurtin, 2003).

Considering higher order variables, introduced as the work conjugate to the gradient of effective strain as done by Shu et al. (Shu et al., 2001), the virtual power balance is written for a body *V*.

$$\int_V \sigma_{ij,j}\delta\dot{u}_i dV + \int_{\partial V}\left(T_i - \sigma_{ij}n_j\right)\delta\dot{u}_i dS + \int_V \left(\tau_{ij}N_{ij} - R + Q_{k,k}\right)\delta\dot{p}dV + \int_{\partial V}\left(m - Q_k n_k\right)\delta\dot{p}dS = 0 \qquad (46)$$

In this expression *N* is the flow direction, *R* represents the nonlocal dislocation drag stress related to isotropic hardening, and *Q* is the higher order nonlocal work conjugate of the effective strain gradient. This virtual power balance expression is based on the concept that power expended can be associated with a force system; therefore, independent treatment of the coupling of the nonlocal variables may not be needed.

Following the usual treatment, the boundary conditions can be determined from the virtual power balance expression by requiring that variational displacement and effective strain (*u* and *p*) may be arbitrarily specified. On the macroscopic level the classical boundary conditions remain unchanged:

$$\sigma_{ij,i} = 0 \text{ and } T_i = \sigma_{ij}n_j \qquad (47)$$

Additionally two nonlocal boundary conditions also appear: the nonlocal microforce condition

$$\tau_{ij} N_{ij} = R - Q_{k,k} \tag{48}$$

and the microtraction bound condition

$$m = Q_k n_k \tag{49}$$

The nonlocal microforce boundary condition may be considered as the nonlocal yield condition, following Gurtin (Gurtin, 2003), and a nonlocal application of the Clausius-Duhmen inequality may be used demonstrate thermodynamic admissibility of the associated constitutive equations (Abu Al-Rub et al., 2007). The microtraction boundary condition is considered to represent the interaction of long-range dislocation forces across interfaces, such as the grain boundaries.

The use of a C^1 formulation to incorporate the effects of long-range dislocations into the CDD model is proposed as a solution to the numerical challenges and mathematical limitations of the C^0 formulation currently employed within the WSU ABAQUS UMAT subroutine. Although this proposed C1 formulation is not without its own numerical implementation concerns, the potential to capture the effects of long range GND densities is exciting

ACKNOWLEDGEMENTS

This work was funded by DOE's Nuclear Energy Advanced Modeling and Simulation (NEAMS) program at Pacific Northwest National Laboratory (PNNL). PNNL is operated by Battelle for the DOE under contract No. DE-AC05-76RL01830.

REFERENCES

Abu Al-Rub, R.K., Voyiadjis, G.Z., Aifantis, E.C., 2009. On the thermodynamics of higher-order gradient plasticity for size-effects at the micron and submicron length scales. International Journal of Materials & Product Technology 34, 172-187.

Abu Al-Rub, R.K., Voyiadjis, G.Z., Bammann, D.J., 2007. A thermodynamic based higher-order gradient theory for size dependent plasticity. International Journal of Solids and Structures 44, 2888-2923.

Acharya, A., Bassani, J.L., 2000. Lattice incompatibility and a gradient theory of crystal plasticity. Journal of the Mechanics and Physics of Solids 48, 1565-1595.

Alankar, A., Field, D.P., Zbib, H.M., 2012a. Explicit incorporation of cross-slip in a dislocation density-based crystal plasticity model. Philosophical Magazine 92, 3084-3100.

Alankar, A., Mastorakos, I.N., Field, D.P., Zbib, H.M., 2012b. Determination of Dislocation Interaction Strengths Using Discrete Dislocation Dynamics of Curved Dislocations. Journal of Engineering Materials and Technology 134, 021018.

Arnold, S., Saleeb, A.F., 1994. On the thermodynamic framework of generalized coupled thermoelastic-viscoplastic-damage modeling. International Journal of Plasticity 10, 263-278.

Arsenlis, A., Parks, D.M., 1999. Crystallographic aspects of geometrically-necessary and statistically-stored dislocation density. Acta Materialia 47, 1597-1611.

Arsenlis, A., Parks, D.M., 2002. Modeling the evolution of crystallographic dislocation density in crystal plasticity. Journal of the Mechanics and Physics of Solids 50, 1979-2010.

Asaro, R.J., 1983. Micromechanics of crystals and polycrystals. Advances in applied mechanics 23, 1-115.

Asaro, R.J., Needleman, A., 1985. Texture development and strain hardening in rate dependent polycrystals. Acta metallurgica 33, 923-953.

Asaro, R.J., Rice, J., 1977. Strain localization in ductile single crystals. Journal of the Mechanics and Physics of Solids 25, 309-338.

Bassani, J.L., 2001. Incompatibility and a simple gradient theory of plasticity. Journal of the Mechanics and Physics of Solids 49, 1983-1996.

Bitzek, E., Brandl, C., Derlet, P., Van Swygenhoven, H., 2008. Dislocation cross-slip in nanocrystalline fcc metals. Physical review letters 100, 235501.

Bonny, G., Pasianot, C., Malerba, L., 2009. e-Ni many-body potential for metallurgical applications. Modelling and Simulation in Materials Science and Engineering 17, 075005.

Busso, E.P., Meissonnier, F.T., O'Dowd, N.P., 2000. Gradient-dependent deformation of two-phase single crystals. Journal of the Mechanics and Physics of Solids 48, 2333-2361.

Canova, G., Brechet, Y., Kubin, L.P., Devincre, B., Pontikis, V., Condat, M., 1993. 3D Simulation of Dislocation Motion on a Lattice: Application to the Yield Surface of Single Crystals. Microstructures and Physical Properties (ed. J. Rabiet), CH-Transtech.

Daw, M., Baskes, M., 1983. Embedded-atom method: Derivation and application to impurities, surfaces, and other defects in metals. Physical Review B 29, 6443-6453.

De Borst, R., Pamin, J., 1996. SOME NOVEL DEVELOPMENTS IN FINITE ELEMENT PROCEDURES FOR GRADIENT-DEPENDENT PLASTICITY. International Journal for Numerical Methods in Engineering 39, 2477-2505.

Devincre, B., Hoc, T., Kubin, L., 2008. Dislocation mean free paths and strain hardening of crystals. Science 320, 1745-1748.

Diaz de la Rubia, T., Zbib, H.M., Victoria, M., Wright, A., Khraishi, T., Caturla, M., 2000. Flow Localization in Irradiated Materials: A Multiscale Modeling Approach. Nature 406, 871-874.

Evans, A.G., Hutchinson, J.W., 2009. A critical assessment of theories of strain gradient plasticity. Acta Materialia 57, 1675-1688.

Evers, L.P., Brekelmans, W.A.M., Geers, M.G.D., 2004. Non-local crystal plasticity model with intrinsic SSD and GND effects. Journal of the Mechanics and Physics of Solids 52, 2379-2401.

Fleck, N., Hutchinson, J., 1993. A phenomenological theory for strain gradient effects in plasticity. Journal of the Mechanics and Physics of Solids 41, 1825-1857.

Fleck, N., Hutchinson, J., 1997. Strain gradient plasticity. Advances in applied mechanics 33, 295-361.

Fleck, N., Muller, G., Ashby, M., Hutchinson, J., 1994. Strain gradient plasticity: theory and experiment. Acta Metallurgica et Materialia 42, 475-487.

Fleck, N., Willis, J., 2009a. A mathematical basis for strain-gradient plasticity theory—Part I: Scalar plastic multiplier. Journal of the Mechanics and Physics of Solids 57, 161-177.

Fleck, N., Willis, J., 2009b. A mathematical basis for strain-gradient plasticity theory. Part II: Tensorial plastic multiplier. Journal of the Mechanics and Physics of Solids 57, 1045-1057.

Gao, H., Huang, Y., Nix, W.D., Hutchinson, J.W., 1999. Mechanism-based strain gradient plasticity— I. Theory. Journal of the Mechanics and Physics of Solids 47, 1239-1263.

Ghoniem, N.M., Singh, B.N., Sun, L.Z., de la Rubia, T.D., 2000. Interaction and accumulation of glissile defect clusters near dislocations. Journal of Nuclear Materials 276, 166-177.

Ghoniem, N.M., Sun, L., 1999. A Fast Sum Method for the Elastic Field of 3-D Dislocation Ensembles. Phys. Rev. B, 60, 128-140.

Gilbert, M., Queyreau, S., Marian, J., 2011. Stress and temperature dependence of screw dislocation mobility in α-Fe by molecular dynamics. Physical Review B 84, 174103.

Groh, S., Marin, E., Horstemeyer, M., Zbib, H., 2009. Multiscale modeling of the plasticity in an aluminum single crystal. International Journal of Plasticity 25, 1456-1473.

Gurtin, M.E., 2000. On the plasticity of single crystals: free energy, microforces, plastic-strain gradients. Journal of the Mechanics and Physics of Solids 48, 989-1036.

Gurtin, M.E., 2003. On a framework for small-deformation viscoplasticity: free energy, microforces, strain gradients. International Journal of Plasticity 19, 47-90.

Guyot, P., Dorn, J.E., 1967. A critical review on the Peierls mechanism. Can. J. Phys. 45, 983-1016.

Henshall, G., 1996. Improvement in the MATMOD equations for modeling solute effects and yield-surface distortion. Unified Constitutive Laws of Plastic Deformation. Academic Press, Inc, 6277 Sea Harbor Dr, Orlando, FL 32887-4900, USA, 1996., 153-227.

Hill, R., 1966. Generalized constitutive relations for incremental deformation of metal crystals by multislip. Journal of the Mechanics and Physics of Solids 14, 95-102.

Hiratani, M., Bulatov, V., Zbib, H.M., 2004. Orientation dependent elastic interaction between a truncated stacking fault tetrahedron and a glissile dislocation. . J. Nuc. Materials, *329-333*, 1103-1106.

Hiratani, M., Zbib, H.M., Khaleel, M.A., 2002a. Modeling of Thermally Activated Dislocation Glide and Plastic Flow through Local Obstacles. Int. J. Plasticity 19, 1271-1296.

Hiratani, M., Zbib, H.M., Wirth, B., 2002b. Interaction of Glissele Dislocations with Perfect and Truncated Stacking Fault Tetraherda in Irradiated Materials. Phil Mag. 82, 2709-2735.

Hochrainer, T., Zaiser, M., Gumbsch, P., 2007. A three-dimensional continuum theory of dislocation systems: kinematics and mean-field formulation. Philosophical Magazine 87, 1261-1282.

Huang, Y., Qu, S., Hwang, K.C., Li, M., Gao, H., 2004. A conventional theory of mechanism-based strain gradient plasticity. International Journal of Plasticity 20, 753-782.

Hutchinson, J., 1976. Bounds and self-consistent estimates for creep of polycrystalline materials. Proceedings of the Royal Society of London. A. Mathematical and Physical Sciences 348, 101-127.

Jackson, P., 1985. Dislocation modelling of shear in fcc crystals. Progress in materials science 29, 139-175.

Keh, A.S., 1965. Work hardening and deformation sub-structure in iron single crystals deformed in tension at 298K. Philosophical Magazine 12, 9-30.

Khraishi, T., Zbib, H.M., Diaz de la Rubia, T., Victoria, M., 2002a. Localized Deformation and Hardening In Irradiated Metals: Three-Dimensional Discrete Dislocation Dynamics Simulations,. Metall. Mater. Trans. 33B, 285-296.

Khraishi, T.A., Zbib, H.M., De La Rubia, T.D., Victoria, M., 2002b. Localized deformation and hardening in irradiated metals: Three-dimensional discrete dislocation dynamics simulations. Metallurgical and Materials Transactions B-Process Metallurgy and Materials Processing Science 33, 285-296.

Kocks, U.F., 1976. Laws for work-hardening and low-temperature creep. Journal of Engineering Materials and Technology-Transactions of the Asme 98, 76-85.

Lebensohn, R., Tomé, C., 1993. A self-consistent anisotropic approach for the simulation of plastic deformation and texture development of polycrystals: application to zirconium alloys. Acta Metallurgica et Materialia 41, 2611-2624.

Lebensohn, R., Tomé, C., 1994. A self-consistent viscoplastic model: prediction of rolling textures of anisotropic polycrystals. Materials Science and Engineering: A 175, 71-82.

Lebensohn, R.A., and Tome, C. N. , 1991. Modelling Twinning in Texture Development Codes. Textures and Microstructures 14-18, 959-964.

Lee, M., Lim, H., Adams, B., Hirth, J., Wagoner, R., 2010a. A dislocation density-based single crystal constitutive equation. International Journal of Plasticity 26, 925-938.

Lee, M.G., Lim, H., Adams, B.L., Hirth, J.P., Wagoner, R.H., 2010b. A dislocation density-based single crystal constitutive equation. International Journal of Plasticity 26, 925-938.

Lequeu, P., Gilormini, P., Montheillet, F., Bacroix, B., Jonas, J., 1987. Yield surfaces for textured polycrystals--I. Crystallographic approach. Acta metallurgica 35, 439-451.

Li, D.S., Zbib, H., X., S., M., K., in preparation. Mechanism based Continuum Dislocation Dynamics with Application on Plastic Flow and Irradiation Hardening of Single Crystal Iron. International Journal of Plasticity.

Li, D.S., Zbib, H.M., Garmestani, H.S., Khaleel, M., Sun, X., 2010. Modeling of irradiation hardening of Polycrystalline Materials. Comp. Mater. Sci. 50, 2496-2501.

Lim, H., Lee, M.G., Kim, J.H., Adams, B.L., Wagoner, R.H., 2011. Simulation of polycrystal deformation with grain and grain boundary effects. International Journal of Plasticity 27, 1328-1354.

Mandel, J., 1965. Généralisation de la théorie de plasticité de WT Koiter. International Journal of Solids and structures 1, 273-295.

Marian, J., Caro, A., 2006. Moving dislocations in disordered alloys: Connecting continuum and discrete models with atomistic simulations. Physical Review B 74, 024113.

Mastorakos, I., Le, L., Zeine, M., Zbib, H.M., Khaleel, M., 2010. Multiscale Modeling of irradiation induced hardening. In: a-Fe, Fe-Cr and Fe-Ni Systems. In: a-Fe, Fe-Cr and Fe-Ni Systems, in *Basic Actinide Science and Materials for Nuclear Applications*, in: J.K. Gibson, S.K.M., E.D. Bauer, L. Soderholm, T. Fanghaenel, R. Devanathan, A. Misra, C. Trautmann, B.D. Wirth (Ed.), MRS. MRS.

Mastorakos, I., Zbib, H.M., Khaleel, M., 2011a. The effect of copper and nickel concentration on the mobility of edge dislocations in Fe alloys. Mat Sc Eng A submitted.

Mastorakos, I., Zbib, H.M., Khaleel, M., 2011b. On the interaction of an edge dislocation with spherical voids in α-Fe and Fe-Ni systems. Computational Materials Science submitted.

Mendelev, M.I., Han, S., Srolovitz, D.J., Ackland, G.J., Sun, D.Y., Asta, M., 2003. Development of new interatomic potentials appropriate for crystalline and liquid iron. Phil Mag 83, 3977-3994.

Miller, A., 1976. An inelastic constitutive model for monotonic, cyclic, and creep deformation: Part I—Equations development and analytical procedures. Journal of Engineering Materials and Technology 98, 97.

Muhlhaus, H.B., Aifantis, E.C., 1991. The influence of microstructure-induced gradients on the localization of deformation in viscoplastic materials. Acta Mechanica 89, 217-231.

Nadgorny, E., 1988. *Dislocation Dynamics and Mechanical Properties of Crystals*. Pergamon Press, Oxford.

Nye, J.F., 1953. Some geometrical relations in dislocated crystals. Acta Metallurgica 1, 153-162.

Ohashi, T., 1994. Numerical modeling of plastic multislip in metal crystals of fcc type. Philos. Mag. A-Phys. Condens. Matter Struct. Defect Mech. Prop. 70, 793-803.

Ohashi, T., Kawamukai, M., Zbib, H., 2007. A multiscale approach for modeling scale-dependent yield stress in polycrystalline metals. International Journal of Plasticity 23, 897-914.

Orowan, E., 1940. Problems of plastic gliding. Proceedings of the Physical Society 52, 8.

Ortiz, M., Repetto, E., Stainier, L., 2000. A theory of subgrain dislocation structures. Journal of the Mechanics and Physics of Solids 48, 2077-2114.

Peeters, B., Kalidindi, S., Van Houtte, P., Aernoudt, E., 2000. A crystal plasticity based work-hardening/softening model for bcc metals under changing strain paths. Acta materialia 48, 2123-2133.

Peirce, D., Asaro, R., Needleman, A., 1982. An analysis of nonuniform and localized deformation in ductile single crystals. Acta metallurgica 30, 1087-1119.

Polizzotto, C., Borino, G., Fuschi, P., 1998. A thermodynamically consistent formulation of nonlocal and gradient plasticity. Mechanics Research Communications 25, 75-82.

Püschl, W., 2002. Models for dislocation cross-slip in close-packed crystal structures: a critical review. Progress in materials science 47, 415-461.

Rashid, M.M., 1993. Incremental kinematics for finite element applications. International Journal for Numerical Methods in Engineering 36, 3937-3956.

Rhee, M., Zbib, H., Hirth, J., Huang, H., De la Rubia, T., 1999. Models for long-/short-range interactions and cross slip in 3d dislocation simulation of bcc single crystals. Modelling and Simulation in Materials Science and Engineering 6, 467.

Roters, F., Eisenlohr, P., Hantcherli, L., Tjahjanto, D.D., Bieler, T.R., Raabe, D., 2010. Overview of constitutive laws, kinematics, homogenization and multiscale methods in crystal plasticity finite-element modeling: Theory, experiments, applications. Acta Materialia 58, 1152-1211.

Sandfeld, S., Hochrainer, T., Zaiser, M., Gumbsch, P., 2011. Continuum modeling of dislocation plasticity: Theory, numerical implementation, and validation by discrete dislocation simulations. Journal of Materials Research 26, 623-632.

Schoenfeld, S., Ahzi, S., Asaro, R., 1995. Elastic-plastic crystal mechanics for low symmetry crystals. Journal of the Mechanics and Physics of Solids 43, 415-446.

Shu, D.J., Liu, F., Gong, X.G., 2001. Simple generic method for predicting the effect of strain on surface diffusion. Physical Review B 64, 245410.

Simo, J.C., Taylor, R.L., 1985. Consistent tangent operators for rate-independent elastoplasticity. Computer methods in applied mechanics and engineering 48, 101-118.

Stelmashenko, N., Walls, M., Brown, L., Milman, Y.V., 1993. Microindentations on W and Mo oriented single crystals: an STM study. Acta Metallurgica et Materialia 41, 2855-2865.

Stukowski, S., Sadigh, B., Erhart, P., Caro, A., 2009. Efficient implementation of the concentration-dependent embedded atom method for molecular-dynamics and Monte-Carlo simulations. Modelling and Simulation in Materials Science and Engineering, 17, 075005.

Tiem, S., Berveiller, M., and Canova, G. R., 1986. Grain Shape Effects on the Slip System Activity and on the Lattice Rotations. Acta Metall. 34, 2139-2149.

Tome, C.N., Lebensohn, R. A., and Kocks, U. F., 1991. A Model for Texture Development Dominated by Deformation Twinning: Application to Zirconium Alloys. Acta Metallurgica 39, 2667.

Tonks, M., 2012. MARMOT Theory Manual. Idaho National Laboratory.

Zbib, H., Li, D., Sun, X., Khaleel, M.A., 2012. Large Scale DD Simulation Results for Crystal Plasticity Parameters in Fe-Cr and Fe-Ni Systems. Pacific Northwest National Laboratory.

Zbib, H.M., Aifantis, E.C., 1992. On the gradient-dependent theory of plasticity and shear banding. Acta Mechanica 92, 209-225.

Zbib, H.M., Aifantis, E.C., 2003. Size effects and length scales in gradient plasticity and dislocation dynamics. Scripta Materialia 48, 155-160.

Zbib, H.M., de la Rubia, T.D., 2002. A multiscale model of plasticity. International Journal of Plasticity 18, 1133-1163.

Zbib, H.M., de La Rubia, T.D., Rhee, M., Hirth, J.P., 2000. 3D Dislocation Dynamics: Stress-Strain behavior and Hardening Mechanisms in FCC and BCC Metals. J. Nuc. Maters 276, 154-165.

Zbib, H.M., Diaz de la Rubia, T., 2002. A multiscale model of plasticity. International Journal of Plasticity 18, 1133-1163.

Zbib, H.M., Rhee, M., Hirth, J.P., 1996. 3D Simulation of Curved Dislocations: Discretization and Long Range Interactions. Advances in Engineering Plasticity and its Applications, eds. T. Abe and T. Tsuta. Pergamon, NY, 15-20.

Zbib, H.M., Rhee, M., Hirth, J.P., 1998. On plastic deformation and the dynamics of 3D dislocations. International Journal of Mechanical Sciences 40, 113-127.

Zhang, L., Tonks, M.R., Gaston, D., Peterson, J.W., Andrs, D., Millett, P.C., Biner, B.S., 2013. A quantitative comparison between and elements for solving the Cahn–Hilliard equation. Journal of Computational Physics 236, 74-80.